

# Explanations Go Linear: Interpretable and Individual Latent Encoding for Post-hoc Explainability

Simone Piaggese *University of Pisa, Pisa, Italy, simone.piaggese@di.unipi.it*  
 Riccardo Guidotti *University of Pisa and ISTI-CNR, Pisa, Italy, riccardo.guidotti@unipi.it*  
 Fosca Giannotti *Scuola Normale Superiore, Pisa, Italy, fosca.giannotti@sns.it*  
 Dino Pedreschi *University of Pisa, Pisa, Italy, dino.pedreschi@unipi.it*

**Abstract**—Post-hoc explainability is essential for understanding black-box machine learning models. Surrogate-based techniques are widely used for local and global model-agnostic explanations but have significant limitations. Local surrogates capture non-linearities but are computationally expensive and sensitive to parameters, while global surrogates are more efficient but struggle with complex local behaviors. In this paper, we present ILLUME, a flexible and interpretable framework grounded in representation learning, that can be integrated with various surrogate models to provide explanations for any black-box classifier. Specifically, our approach combines a globally trained surrogate with instance-specific linear transformations learned with a meta-encoder to generate both local and global explanations. Through extensive empirical evaluations, we demonstrate the effectiveness of ILLUME in producing feature attributions and decision rules that are not only accurate but also robust and faithful to the black-box, thus providing a unified explanation framework that effectively addresses the limitations of traditional surrogate methods.

## I. INTRODUCTION

Explainable AI (XAI) refers to a well-established set of methodologies devised to help humans build interpretable Machine Learning (ML) prediction pipelines. Within XAI, model-agnostic *post-hoc* explainability [1], [2] comprehends a broad range of algorithms developed to generate *explanations* for “black-box” models. Explanations can take various forms, with the most commonly used and studied being feature attribution, decision rules, and counterfactuals [1], [3]. Black-box explanations aim to shed light on AI decision-making process at both the local and global levels. Among post-hoc explanation techniques, surrogate explainers are largely adopted given their effectiveness in performing complex model distillation [4], [5]. Global surrogates, like TREPAN [6] and related approaches [5], involve training a single interpretable model (e.g., linear regression or decision tree) to replicate the behavior of the target predictor, thus providing a comprehensive understanding of the black-box across the entire dataset. Given their simplicity, global surrogates may struggle to capture highly non-linear relationships, potentially resulting in poor generalization and insufficiently informative explanations. Instead, local surrogates, such as LIME [7] and LORE [8], focus on accurately identifying the factors that influence a specific prediction. They achieve this by training an interpretable model within a (typically synthetically generated) neighborhood of the instance, locally approximating the complex decision boundary of the black-box model. The XAI community largely agrees with identifying local post-hoc explainers as pivotal solutions

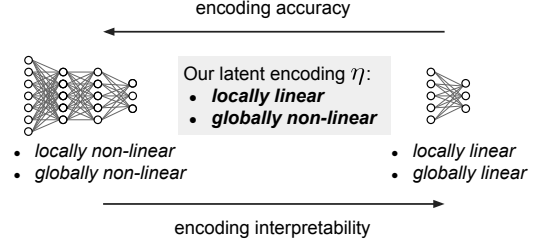


Fig. 1: Accuracy-interpretability trade-off for feed-forward neural architectures for latent encoding.

for explainability [1], [2]. Despite their success, existing local explanation methods face several limitations [9]–[11], including instability of explanations [12], [13], high sensitivity to hyper-parameters [14], [15], computation inefficiencies [16], misleading behaviors [17], [18], and design tailored with the explanation type which limits their flexibility [7], [19]. These challenges are primarily attributed to the biases and sampling variability introduced by the neighborhood generation process [20], [21].

In this work, we bridge the gap between local and global surrogate methods by providing a comprehensive post-hoc explanation framework that: (i) overcomes the restrictions of global surrogates regarding their generalization capabilities, (ii) addresses the methodological issues of local surrogates going beyond neighborhood sampling, and (iii) supports any type of explanation format. To this aim, we combine the predictive modeling capabilities of surrogate estimators with the representational power of neural encoding models [22]–[24]. Our proposed framework redefines the post-hoc explanation problem by operating in a feature space distinct from the input. It transforms the data into a latent representation that enhances the expressiveness of global surrogate explanations. Specifically, we argue that *local explanations can be obtained from (global) latent surrogate-based explanations if the latent mappings are done with locally linear transformations* [25].

Typically, latent mappings [26], [27] are produced by highly non-linear operations, such as Neural Networks (NNs), and present opaque and uninterpretable features, rendering any surrogate explanations that rely on these features ineffective. Conversely, creating interpretable embeddings is inherently challenging [28]–[30] and requires balancing accuracy with transparency [31]. The most straightforward interpretable

embeddings are achieved through linear transformations, e.g., implemented as single-layer NNs [32]–[34] without non-linear activations. As shown in Figure 1, linear NNs (on the right) can be seen as interpretable considering the single-layer structure and the additive nature of output neurons when activation functions are not used. However, at the same time, they are also too restrictive due to their overly simplified architecture [35]. Specifically, they provide interpretable transformations both globally, since the single-layer network defines a linear function with its unique weights matrix  $W$ , and locally, since it applies linearly on each specific instance  $\mathbf{x}$ , resulting in the latent representation  $\mathbf{z} = W\mathbf{x}$ . In contrast, deep NNs achieve greater accuracy but are not interpretable, because applying  $NN(\mathbf{x})$  involves obscure complex and stacked (global and local) nonlinear operations. Neural Additive Models (NAMs) [36] are possible candidates for balancing this trade-off. NAMs define the mapping as a sum of non-linear functions  $NN_j(x_j)$ , for each feature  $j$ , possibly including feature interactions  $NN_{jj'}(x_j, x_{j'})$  [37]. NAMs are human-readable by looking at visual plots of  $NN_j$ s and  $NN_{jj'}$ s [36]. However, assuming only pairwise interactions, NAMs are restrictive and higher-order extensions lose interpretability and scalability. Still, they remain non-linear both locally and globally.

As an alternative solution to balance the trade-off, we introduce **locally-linear transformations** as non-linear maps  $\eta$ , such that  $\mathbf{z} = \eta(\mathbf{x}) = f(\mathbf{x}) \cdot \mathbf{x}$ , where  $f$  is a NN-based function returning a specific weight matrix once applied to any instance  $\mathbf{x}$ . We see that the output of the function  $\eta$  is linear when applied on instance  $\mathbf{x}$ , without being a linear model as a whole (globally not linear). Intuitively,  $f$  acts as a *meta*-encoder, returning for each instance a proper linear encoding used to transform the instance itself.

To exemplify how this architecture redefines the landscape of surrogate-based explanations, we examine the case of feature importance tabular explainers, focusing specifically on additive attribution methods [38]. Given an instance  $\mathbf{x} = \{x_1, \dots, x_m\}$ , where  $x_j$  is the value of  $j$ -th feature in  $\mathbf{x}$ , in local additive explainers, like LIME [7] and SHAP [16], the decision function of a black-box model  $b(\mathbf{x})$  is locally approximated by a sum of feature importance scores  $b(\mathbf{x}) \approx \sum_j \psi_j^x x_j$  where each term  $\psi_j^x$  represents the contribution of feature  $j$  to the prediction for instance  $\mathbf{x}$ . Similarly to additive explainers, training a logistic regression as global surrogate enables an additive expression of the log-odds ratio of predictions [39]  $\log \frac{b(\mathbf{x})}{1-b(\mathbf{x})} \approx \sum_j \beta_j x_j$ . Since weights  $\{\beta_j\}$  are constant, the resulting explanation lacks the expressiveness to convey adequate local knowledge about the black-box, resulting insufficiently informative. On the other hand, if we map the input instances into  $\mathbf{z} = f(\mathbf{x}) \cdot \mathbf{x}$ , we can show that the log-odds ratio of the latent regressor  $\sum_r \beta_r z_r$ , where  $z_r$  is the value of  $r$ -th feature in  $\mathbf{z}$ , can be expressed in the input feature spaces as  $\log \frac{b(\mathbf{x})}{1-b(\mathbf{x})} \approx \sum_j \psi_j^{f(\mathbf{x})} x_j$ . The property of  $f$  being locally linear ensures that we can reconstruct the local explanation in terms of the original features from the latent surrogate explanations. The same approach illustrated here for feature attribution can be similarly applied to any type of surrogate explanations, including factual and counterfactual

rules returned by LORE [8] or decision trees adopted as global surrogates like in TREPAN [6].

Based on the idea of local linear transformations, we introduce ILLUME, an Interpretable individual Latent neUral Mapping for Explainability. ILLUME is designed to learn a locally-linear latent encoding, thus interpretable and tailored to any specific instance, to generate local explanations from surrogate models that globally approximate the behavior of any black-box decision-making system. Specifically, we show how to constrain the latent space encoding such that the resulting explanations meet desirable properties. With ILLUME, we aim to achieve the precision of post-hoc local explainers, while maintaining the efficiency and simplicity of global surrogate models. Also, the latent encoding is agnostic with respect to the surrogate model, enabling the extraction of different types of explanations. With a wide range of experiments on tabular data, we show that ILLUME is able to generate local explanations as feature importance and decision rules, leading to more accurate, robust, faithful, and efficient explanations than state-of-the-art methods.

The rest of the paper is organized as follows. After reviewing related literature in Section II, we describe ILLUME in Sec. III. In Sec. IV, we present the experimental results. Finally, Sec. V summarizes our contributions and outlines potential directions for future research.

## II. RELATED WORKS

To frame our proposal, we present a brief review on surrogate-based methods, feature projection, and representation learning for XAI.

Surrogate explainability methods approximate black-box model predictions using simple interpretable models [40]. Global surrogates aim to capture the overall decision logic of the black-box through model distillation [4]–[6]. On the other hand, local surrogates focus on specific model decisions. LIME [7] and subsequent improvements [41], [42] computes feature importance using linear models on locally sampled neighborhoods, while LORE [8], [43] extracts logic rules with locally trained decision trees, enhancing neighborhood generation with genetic algorithms. Other works connecting game theory with local explanations, such as SHAP [44], enable model-agnostic estimation of Shapley values with local surrogate models. Alternatively, methods like GLOCALX [45] hierarchically merge local surrogate explanations to globally emulate the black-box. Global surrogates can be more efficient than local ones but they might miss complex non-linear relationships of the black-box models [5], [6]. In contrast, local surrogates better capture non-linear decision boundaries but can be unstable [12], [13], sensitive to hyperparameters [14], [15], and computationally demanding [16].

Various XAI methods train surrogate models by leveraging feature projection techniques [46]. Among these, we can distinguish dimensionality reduction [47] and manifold learning. However, these approaches are typically used to visualize high-dimensional data by optimizing low-dimensional representations. Among them, methods such as PCA [19] and MDS [48] were designed to preserve the overall structure of the data.

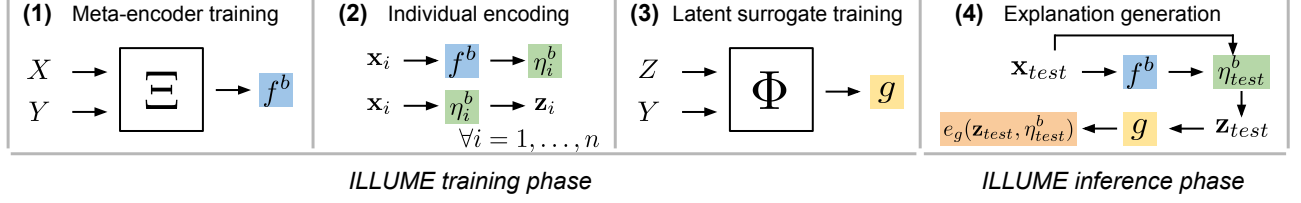


Fig. 2: ILLUME steps: (1) the meta-encoder  $f^b$  is trained using input instances  $X$  and black-box decisions  $Y$ ; (2)  $f^b$  generates specific encoding functions  $\eta_i^b$  to individually map instances  $\mathbf{x}_i$  into latent representations  $\mathbf{z}_i$ ; (3) the set of latent vectors  $Z$  is used to train a surrogate model  $g$  for imitating the black-box  $Y = b(X)$ ; (4) given a test instance  $\mathbf{x}_{test}$ , it is mapped into  $\mathbf{z}_{test}$  with  $\eta_{test}^b$  obtained by  $f^b$ , then the explanation is obtained with  $e_g(\mathbf{z}_{test}, \eta_{test}^b)$  by combining the surrogate logic  $g$  with local mapping  $\eta_{test}^b$ . Training algorithms are marked with white squares. Learned functions are marked with different colored boxes.

Later, more sophisticated techniques such as ISOMAP [49] and LLE [50] were developed to capture local relationships often overlooked by global techniques. More recently, algorithms like T-SNE [27] and UMAP [51] have gained widespread popularity across scientific disciplines due to their ability to efficiently maintain local complexities and non-linear patterns. However, the embeddings produced by these techniques are opaque, preventing their direct usage in XAI contexts, as they rely on complex, non-linear transformations. Consequently, there is growing interest in better understanding embedding representations [52]–[54], or learning inherently interpretable ones [32], [34], [55].

Representation learning involves techniques for automatically deriving feature encoding functions from data [22], [56]. It has become a fundamental component of NN-based models, enabling a wide range of tasks including generative methods [57], [58], classification [59], [60], and regression [36], [61]. In XAI, latent space methods usually employ deep architectures like (auto-)encoders, to generate explanations such as exemplars [62]–[64] and counterfactuals [65], [66], without looking at the transparency of the entire process. Alternatively, interpretable latent spaces have been proposed [32], [34] to facilitate counterfactual search, though their expressive power is limited by global linear mappings. Moreover, approaches that jointly train neural encoders with explanation generators have been developed to create self-explaining models [67]–[69], offering an alternative to post-hoc, model-agnostic explainability methods. While these self-explaining models provide robust explanatory capabilities, they are not designed for post-hoc explainability, which limits their usability.

Our proposal addresses the limitations of the approaches above by creating an encoding function that is both expressive and interpretable. This function enables the reformulation of local explanations using only globally trained surrogates.

### III. METHODOLOGY

We define here ILLUME, a procedure to train an interpretable latent space model that enable learning global post-hoc surrogates to approximate black-box systems in a transparent way. We first outline the problem formulation and the design principles. Then we provide the details of the interpretable encoding model and the required regularization terms. Finally, we describe the procedure that leverages the interpretable encoding to realize the explanation generator.

#### A. Problem Setting and Proposed Approach

Given an input space  $\mathcal{X} \subseteq \mathbb{R}^m$  where  $m$  is the number of features, let  $X = \{\mathbf{x}_1, \dots, \mathbf{x}_n\}$  denote a dataset of  $n$  instances in  $\mathcal{X}$ . Each instance  $\mathbf{x}_i = (x_{i,1}, \dots, x_{i,m})$  consists of  $m$  feature values, where  $x_{i,j}$  represents the value of the  $j$ -th feature in  $\mathbf{x}_i$ . We define a black-box predictor trained on  $X$ ,  $b: \mathcal{X} \rightarrow \mathcal{Y}$ , where  $\mathcal{Y}$  is the codomain of the black-box. We focus here on classification tasks, where  $\mathcal{Y} \subset [0, 1]^c$  and  $c$  denotes the number of classes. Typically, the black-box outputs probability estimates for each class, i.e.,  $c = 2$  corresponds to binary classification problems, while  $c > 2$  applies to multi-class problems<sup>1</sup>. Local explanations of black-box  $b$  are the output of functions  $e^b: \mathcal{X} \rightarrow \mathcal{E}$ , where  $\mathcal{E}$  is the space of explanations. Given an instance  $\mathbf{x}_i$ , a local explainer optimizes a function  $e_i^b$  that returns  $e_i^b(\mathbf{x}_i)$  as explanation, to highlight the factors that activate black-box decision  $b(\mathbf{x}_i)$ .

Given the pair  $(X, Y)$ , where  $Y = \{b(\mathbf{x}_1), \dots, b(\mathbf{x}_n)\}$  denotes the predictions of the black-box  $b$  on  $X$ , the objective of ILLUME is to fit a single *explanation generator*  $e_g$  that, given any instance  $\mathbf{x}_{test}$ , is able to explain the decision  $b(\mathbf{x}_{test})$ . Thus, instead of returning an independent explainer  $e_i^b$  for each instance like for local surrogates, ILLUME produces a single ML function  $e_g$  that individually adapts to the instances analyzed. Such a post-hoc explanation generator offers superior advantages over inherently local explainers. As an inductive function, the generator has more generalization capabilities over local surrogates, which require training an independent model for each instance. Additionally, as model parameters are shared among instances in the population, ILLUME is equipped with a global view of the explained black-box [70]. Also, by retraining for every single explanation, local surrogates are impractical for extensive interpretation tasks.

At the core of ILLUME is the *meta-encoder*. Departing from traditional latent space approaches, such as autoencoders or conditioned autoencoders [60], [71], which directly learn functions  $\mathcal{X} \rightarrow \mathcal{Z}$  or  $(\mathcal{X} \times \mathcal{Y}) \rightarrow \mathcal{Z}$ , we focus on optimizing a more sophisticated class of functions  $f: \mathcal{X} \rightarrow (\mathcal{X} \rightarrow \mathcal{Z})$ . While mimicking classical encoders in the mapping result, proposed meta-encoder optimizes an intermediate space  $\mathcal{W}$ , i.e. the continuous space of linear applications from  $\mathcal{X}$  to  $\mathcal{Z}$ , returning an *individual, locally-linear transformation* for each

<sup>1</sup>Although here we focus on binary classification, our approach can be easily extended to multi-class problems using one-vs-rest classifiers.

instance. Individual and linear maps enhance interpretability through linear combinations of input variables and, being instance-specific, offer more expressive power than usual linear maps. ILLUME’s steps illustrated in Figure 2 are as follows:

- 1) A first optimization algorithm  $\Xi : (\mathcal{X} \times \mathcal{Y}) \rightarrow (\mathcal{X} \rightarrow \mathcal{W})$  trains the meta-encoder  $f : \mathcal{X} \rightarrow \mathcal{W}$  over the conditioned space  $\mathcal{X} \times \mathcal{Y}$ . Being conditioned to the black-box  $b$ , we denote the learned function as  $f^b$ , which returns locally-linear transformations  $\eta_i^b$  for any given instance  $\mathbf{x}_i$ . Each  $\eta_i^b : \mathcal{X} \rightarrow \mathcal{Z}$  maps input space records into a  $k$ -dim latent space, while preserving feature and decision proximities.
- 2) Then, for each instance  $\mathbf{x}_i \in X$ , the trained meta-encoder derives its local-linear transformations  $\eta_i^b = f^b(\mathbf{x}_i)$  that consists in a matrix  $W_i^b \in \mathbb{R}^{m \times k}$ . Such transformations are applied to each instance  $\mathbf{x}_i \in X$ , obtaining the latent embeddings  $\mathbf{z}_i = \eta_i^b(\mathbf{x}_i) = W_i^b \mathbf{x}_i$ .
- 3) Given the dataset of latent instances  $Z = \{\mathbf{z}_1, \dots, \mathbf{z}_n\}$  and the observed black-box decisions  $Y$ , a second optimization  $\Phi : (Z \times \mathcal{Y}) \rightarrow (Z \rightarrow \mathcal{Y})$  is performed to train the *surrogate model*  $g : Z \rightarrow \mathcal{Y}$  that globally approximate the black-box in the latent space  $\mathcal{Z}$ .
- 4) At inference time, given any (also previously unseen) instance  $\mathbf{x}_{test}$ , the locally-linear transformation and the latent representation are obtained as  $W_{test}^b = f^b(\mathbf{x}_{test})$  and  $\mathbf{z}_{test} = W_{test}^b \mathbf{x}_{test} = \eta_{test}^b(\mathbf{x}_{test})$ . The decision of the surrogate is obtained as  $y_{test} = g(\mathbf{z}_{test})$ , while the explanation is extracted from the *explanation generator*  $e_g(\mathbf{z}_{test}, \eta_{test}^b)$  depending on the type of the surrogate by considering the latent representation  $\mathbf{z}_{test}$  and the locally-linear transformation  $\eta_{test}^b$ .

ILLUME constructs explanations according to the chosen surrogate model, e.g., providing feature importance for linear models or factual/counterfactual rules for decision trees. The encoder layer is trained separately from the surrogate, which allows capturing the black-box behavior in a general-purpose meta-model. This modular design enables seamless integration with any surrogate predictor without redesigning the architecture. ILLUME is designed for input data with interpretable features, such as semantically labeled or concept-based attributes typical of tabular datasets. While this may seem restrictive, interpretable feature representations are the backbone of many explainers that target black-box predictive systems [72]. Hence, we focus on explanations for tabular data, which are easier to analyze and understand without conversions.

### B. Principled Design of ILLUME

We outline here the key properties that encoding functions  $\eta : \mathcal{X} \rightarrow \mathcal{Z}$  should satisfy to ensure that any interpretable surrogate predictor is optimized for producing meaningful explanations.

**(P1) Decision Conditioning.** The encoding captures the relationships among the input features  $\mathbf{x}_i$  and the black-box outcomes for each instance  $b(\mathbf{x}_i)$ , thereby aligning the learned representations with the black-box decision boundary [32], [34]. In other words, the encoding  $\eta$  also depends on the local black-box prediction  $b$ , such that  $\mathbf{z}_i = \eta^b(\mathbf{x}_i)$ . This design choice ensures that the surrogate model trained on the interpretable

latent encoding  $\mathcal{Z}$  will capture the behavior of the black-box model it aims to explain.

**(P2) Local Linearity.** The encoding maps linearly the input, by using matrix transformation  $W^b \in \mathbb{R}^{m \times k}$ , such that relationship between the original features and the latent features is human-interpretable [32], [73]. Moreover, instead of using a global transformation  $W^b$  for all instances, we allow each instance to have its own *individual* linear map. Indeed, we aim to derive a set of matrices  $\{W_1^b, \dots, W_n^b\}$ , each of which linearly maps an instance to its corresponding latent representation, i.e.,  $\mathbf{z}_i = \eta_i^b(\mathbf{x}_i) = W_i^b \mathbf{x}_i$ . Specifically,  $z_{i,r} = \sum_{j=1}^m W_{i,j,r}^b x_{i,j}$  where  $W_{i,j,r}$  is the value that models the linear relationship between the  $j$ -th input feature and the  $r$ -th latent feature for the  $i$ -th instance. In this way  $\eta_i^b$  retains the flexibility of a deep architecture, avoiding the loss of expressiveness that arises when using a single globally linear transformation [32], [34].

**(P3) Explanation Consistency.** Individual transformations inform how to map specific instances locally, influencing surrogate predictions and thus the explanation generator. To ensure *consistent* explanations, we must guarantee that similar instances  $\mathbf{x}_1$  and  $\mathbf{x}_2$  receive similar encodings, i.e.,  $W_1$  and  $W_2$  should be close. Specifically, if  $\eta_i^b(\mathbf{x}_i) = W_i^b \mathbf{x}_i$  represents the mapping for  $\mathbf{x}_i$ , then the same transformation should hold for a sufficiently small perturbation applied to the input [68], such that  $\eta_i^b(\mathbf{x}_i + \delta) = W_i^b \mathbf{x}_i + W_i^b \delta$ .

Building on the above principles, ILLUME is inspired by dimensionality reduction [47], learning an encoding to the space  $\mathcal{Z}$ . First, ILLUME incorporates both feature-wise and prediction-wise similarity into the latent space model **(P1)**. Inspired by conditioned training in autoencoders and other recent conditioned approaches in the XAI literature [32], [34], [67], through  $\Xi$ , we optimize  $f^b$  on an augmented space  $\mathcal{X}^{(b)} \subseteq \mathcal{X} \times \mathcal{Y}$ , using the enriched dataset  $X^{(b)} = \{(\mathbf{x}_i, b(\mathbf{x}_i)) | \forall i \in [1, n]\}$  with black-box predictions paired to each instance. Second, ILLUME permits training linear transformations without constraining the encoding architecture to be strictly linear, thereby enhancing its expressive power **(P2)**. In particular, ILLUME supports the use of a shared model to compute individual linear transformations while maintaining the ability to generalize beyond the training instances. We express  $W_i^b = f^b(\mathbf{x}_i)$  to emphasize that the  $i$ -th transformation is an explicit learnable function applied to  $\mathbf{x}_i$ . Third, transformations  $W_i^b$  are enforced to be stable w.r.t. infinitesimal displacements of  $\mathbf{x}_i$  **(P3)**. Intuitively, we demand local Lipschitz continuity [12] to bound  $\|f^b(\mathbf{x}) - W_i^b\|_F$  with  $\Lambda \|\mathbf{x} - \mathbf{x}_i\|$  such that  $\|\mathbf{x} - \mathbf{x}_i\| < \|\delta\|$ , for some constant  $\Lambda \in \mathbb{R}$  and perturbation  $\delta \in \mathbb{R}^m$ . Hence, given  $\mathbf{x}_i$ , we require that  $f^b$  applied to a perturbed instance  $(\mathbf{x}_i + \delta)$  remains nearly identical to the transformation applied to  $\mathbf{x}_i$ . This can be obtained by minimizing  $L^{st} = \frac{1}{n} \sum_i \|J_i - W_i^b\|_F^2$ , where  $J_i \in \mathbb{R}^{m \times k}$  is the Jacobian matrix of the transformation around the data-point  $\mathbf{x}_i$ , with entries  $J_{i,j,r} = \frac{\partial z_{i,r}}{\partial x_j} = W_{i,j,r}^b + \sum_{v=1}^m \frac{\partial W_{i,v,r}^b}{\partial x_j} x_v$  (more details in Appendix D).

Since the surrogate aims to replicate black-box decisions  $b(\mathbf{x}_i)$ , the linear functions  $\eta_i^b$  are designed not to directly accept  $b(\mathbf{x}_i)$  as input argument. This prevents information from leaking from the features to the classification label. Instead, the influence of the black-box is incorporated indirectly through

the loss function, detailed in the following. Conceptually, the training optimization  $\Xi$  conditioned on  $\mathcal{Y}$  takes as input the training instances along with black-box decisions, and returns the trained meta-encoder  $f^b$  that does not require  $\mathcal{Y}$  as input. We underline that this is markedly different than using a function  $f^b$  on the explicit domain  $\mathcal{X} \times \mathcal{Y}$ . Indeed, in our proposal, the dependences from  $\mathcal{Y}$ 's observation are captured implicitly in the optimized weights of the neural function  $f^b$  and not requested at inference time.

### C. Training the Interpretable Meta-encoder

As depicted in Figure 2, the first step of ILLUME is training the function  $\Xi : (\mathcal{X} \times \mathcal{Y}) \rightarrow (\mathcal{X} \rightarrow (\mathcal{X} \rightarrow \mathcal{Z}))$  over the space  $\mathcal{X} \times \mathcal{Y}$  to learn a meta-encoder  $f^b : \mathcal{X} \rightarrow (\mathcal{X} \rightarrow \mathcal{Z})$  that is able to return linear transformations. In other words, we aim to obtain the meta-encoder function  $f^b$  such that, given  $\mathbf{x}_i$ ,  $f^b$  returns a linear mapping  $\eta_i^b : \mathcal{X} \rightarrow \mathcal{Z}$  in the form of a matrix  $W_i^b \in \mathbb{R}^{m \times k}$ , i.e.,  $W_i^b = f^b(\mathbf{x}_i)$  with  $\mathbf{z}_i = \eta_i^b(\mathbf{x}_i) = W_i^b \cdot \mathbf{x}_i$ . In this section, we describe the details of ILLUME to obtain  $f$  by satisfying the design principles discussed.

**Learning Objective.** To learn the meta-encoder  $f^b$ , we enforce that the input pairwise distance distributions,  $P_{\mathcal{X}}$  and  $P_{\mathcal{Y}}$ , mirror the distribution  $P_{\mathcal{Z}}$  over the corresponding latent representations. This requirement forces  $\mathcal{Z}$  to capture the structure of data and black-box decisions in  $\mathcal{X}^{(b)}$ , thus yielding effective embeddings that faithfully incorporate the black-box behavior. Moreover, the introduced latent transformations,  $\{W_i^b\}_{i=1\dots n}$ , modulating the mapping of inputs into the encoding space  $\mathcal{Z}$ , are optimized to prevent their distribution from deviating arbitrarily, by requiring  $P_{\mathcal{W}}$  to stay close to  $P_{\mathcal{Z}}$ . This ensures that also  $P_{\mathcal{W}}$  as well reflects the black-box behavior and feature distribution. The learning objective for the model returning  $f^b$ , then, consists of minimizing the following superposition of Kullback-Leibler divergences:

$$L^{kl} = \frac{1}{n} \sum_i \underbrace{KL_i(P_{\mathcal{X}}||P_{\mathcal{Z}}) + KL_i(P_{\mathcal{Z}}||P_{\mathcal{W}})}_{\text{aligns } P_{\mathcal{Z}} \text{ and } P_{\mathcal{W}} \text{ with } P_{\mathcal{X}}} + \underbrace{KL_i(P_{\mathcal{Y}}||P_{\mathcal{Z}})}_{\text{aligns } P_{\mathcal{Z}} \text{ with } P_{\mathcal{Y}}}$$

where  $KL_i(A||B) = \sum_{j=1}^n A_{i,j} \log \frac{A_{i,j}}{B_{i,j}}$ . Probability distributions are calculated with pairwise similarity between instances  $\mathbf{x}_i, \mathbf{x}_j \in \mathcal{X}$ , black-box predictions  $b(\mathbf{x}_i), b(\mathbf{x}_j) \in \mathcal{Y}$ , latent representations  $\mathbf{z}_i, \mathbf{z}_j \in \mathcal{Z}$ , or individual mappings  $W_i^b, W_j^b \in \mathcal{W}$ , as:

$$S_{i,j}(\Omega) = e^{-d_{\Omega}(i,j)^2} / \sum_{v \neq i} e^{-d_{\Omega}(i,v)^2},$$

where  $d_{\Omega}(\cdot, \cdot)$  denotes a specified distance metric over the space  $\Omega$ . In practice, the similarity  $S_{i,j}$  represents the probability of  $j$  being a neighbor of  $i$  according to a Gaussian distribution centered on  $i$ . This objective encourages distributions  $P_{\mathcal{W}}$  and  $P_{\mathcal{Z}}$  to align with  $P_{\mathcal{X}^{(b)}}$ . Instead of directly matching the mappings  $\{W_i^b\}$  with  $X^{(b)}$ , we align  $\{W_i^b\}$  with the embeddings  $\mathcal{Z}$ . This indirect alignment through  $\mathcal{Z}$  effectively allineates  $\{W_i^b\}$  with  $X^{(b)}$ , as  $\mathcal{Z}$  serves as a compact, denoised abstraction of  $X^{(b)}$ , reducing noise and complexity compared to working directly in  $\mathcal{X}$ . Also, we express the loss as  $L^{kl} = L_x^{kl} + L_y^{kl}$ , emphasizing the term  $L_y^{kl} = \frac{1}{n} \sum_i KL_i(S_{d_{\mathcal{Y}}}||S_{d_{\mathcal{Z}}})$  responsible for conditioning on  $\mathcal{Y}$ .

**Model Regularizations.** We employ latent space regularization to impose additional constraints, ensuring *sparsity*, *orthogonality*, and *non-collinearity*. Inspired by previous work on  $\alpha$ -sparse autoencoders [74], [75], we *sparsify* the transformation matrices  $W_i^b$  into  $sp_{\alpha}(W_i^b)$  by identifying the  $\alpha$  largest weights for each column and setting the other to zero. This mechanism ensure that latent space mapping maintains a linear relationship with a limited number of input features. Moreover, it enables the user to choose the preferred sparsity level  $\alpha$ . Also, to minimize redundancy and ensure that diverse input features contribute to distinct latent dimensions, we apply *soft-orthogonality* constraints [76] between column pairs of the transformation matrices, i.e., we impose to minimize the loss  $L^{so} = \frac{1}{n} \sum_i ||sp_{\alpha}(W_i^b) sp_{\alpha}(W_i^b)^{\top} - \mathbb{1}_k||_F^2$ , with  $\mathbb{1}_k$  the unitary matrix. Finally, to ensure the resulting latent space is composed of minimally correlated variables [17], we optimize the correlation matrix of latent data-points  $C(\mathcal{Z})$ , with entries as the empirical Pearson scores<sup>2</sup>  $C_{r,s} = \frac{1}{n} \sum_i \left( \frac{z_{i,r} - \mu(\mathbf{z}_{:,r})}{\sigma(\mathbf{z}_{:,r})} \right) \left( \frac{z_{i,s} - \mu(\mathbf{z}_{:,s})}{\sigma(\mathbf{z}_{:,s})} \right)$ , denoting with  $\mathbf{z}_{:,r} = \{z_{1,r}, \dots, z_{n,r}\}$  the realizations of the  $r$ -th feature, and with  $\mu(\cdot)$  and  $\sigma(\cdot)$  the empirical average and standard deviation functions. *Non-collinearity* is reached by imposing that correlation matrix is nearly identical to the unitary matrix:  $L^{co} = ||C(\mathcal{Z}) - \mathbb{1}_k||_F^2$ .

**Optimization.** The training of  $\Xi$  to obtain  $f^b$  is optimized using mini-batch gradient minimization with Adam optimizer [78], where the objective function a single batch of training instances is:

$$\mathcal{L}(X, Y, \alpha) = L_x^{kl} + \lambda^y L_y^{kl} + \lambda^{st} L^{st} + \lambda^{so} L^{so} + \lambda^{co} L^{co}$$

Similar to  $\alpha$ -sparse autoencoders [75], we introduce a sparsity scheduling approach over training epochs to avoid ‘‘dead’’ hidden units within the deep neural network architecture of  $\Xi$ . Namely, we begin by pre-training the linear model without sparsity constraints, then gradually increase sparsity linearly to the desired level, and finally fine-tune the resulting sparse model until convergence.

### D. Generating the Explanations

In Figure 2, after the meta-encoder training (1), individual encodings map input instances into latent representations (2), that are used as predictor variables for surrogate model fitting (3). Then, at inference time, the meta-encoder  $f^b$  and the surrogate model  $g$  are combined (4) to produce explanations through the generator function  $e_g : \mathcal{Z} \times \mathcal{W} \rightarrow \mathcal{E}$ . Here, we describe how the function  $e_g$  generates local explanations by exploiting the inner logic of the surrogate and the locally linear structure of the latent space. Notably, local explanations depend on the inherent decision-making mechanism of the interpretable surrogate. It is worth underlining that the representation learning phase is separate and independent from the surrogate training phase. We leave as a future work possible extensions of the latent encoding loss that takes into account also the optimization of the surrogate’s classification.

<sup>2</sup>Non-linear rank-based correlation measures, such as Spearman or Kendall scores, are harder to optimize requiring differentiable sorting algorithms [77].

**Feature Importance-based Explanations.** Given an instance  $\mathbf{x}_i$ , feature importance explainers assign a real-valued vector  $\psi_i = (\psi_{i,1}, \dots, \psi_{i,m})$ , in which every  $\psi_{i,j}$  is the relevance of the  $j$ -th feature for the prediction  $b(\mathbf{x}_i)$ . For example, vector  $\psi^x = (\psi_{age} = -0.2, \psi_{inc} = 0.8, \psi_{edu} = 0.5)$  illustrates the feature importance for the decision to reject the loan application for the instance  $\mathbf{x} = (age = 25, income = 15k, education = high)$ . By learning a logistic classifier over  $Z$ , in ILLUME we first derive explanations expressed on latent encodings in the form of additive feature attributions  $g(\mathbf{z}_i) = \beta_0 + \sum_{r=1}^k \beta_r z_{i,r}$ . Then, by exploiting the linearity of  $\eta_i^b$ , through  $e_g$ , the projected space attributions<sup>3</sup> are converted into input space attributions  $g(\eta_i^b(\mathbf{x}_i)) = \sum_{j=1}^m \psi_{i,j} x_{i,j}$ , with feature importance defined as  $\psi_{i,j} = \sum_{r=1}^k \beta_r W_{i,j,r}^b$ . Hence, in ILLUME the local importance of input feature  $j$  is determined by summing up the global relevances of the latent features  $\{\beta_r\}$  weighted by the magnitudes of the mapping  $W_{i,j,r}^b$ . This weighting reflects how strongly feature  $j$  contributes to each latent feature  $r$  based on the logistic surrogate coefficients. Recalling the example above, suppose that instance  $\mathbf{x}$  is mapped into a 2-dim vector  $(z_1 = W_{age,1}^b x_{age} + W_{inc,1}^b x_{inc}, z_2 = W_{age,2}^b x_{age} + W_{edu,2}^b x_{edu})$  given by a sparse transformation. Hence, after learning the global logistic explanation  $\psi^z = (\beta_1, \beta_2)$ , local feature importance vector values are  $\psi^x = (\psi_{age} = \beta_1 W_{age,1}^b + \beta_2 W_{age,2}^b, \psi_{inc} = \beta_1 W_{inc,1}^b, \psi_{edu} = \beta_2 W_{edu,2}^b)$ .

**Rule-based Explanations.** Given a record  $\mathbf{x}_i$ , a set of decision rules  $\rho_i^x$  explains the black-box decision  $b(\mathbf{x}_i)$  with the logical premises that lead to the decision [8].  $\rho_i^x$  is composed by axis-parallel boolean conditions on feature values in the form  $x_{i,j} \in [l_{i,j}^x, u_{i,j}^x]$ , where  $l_{i,j}^x, u_{i,j}^x$  are lower and upper bound values in the domain of  $x_{i,j}$ , extended with  $\pm\infty$ . For example, the rule  $\rho^x = \{age \leq 20, income \leq 30k, education \leq bachelor\}$  explains the rejection of loan application. In ILLUME, when  $g$  is a decision tree, we first derive global decision rules, determined as root-leaf paths in the decision tree trained over feature space  $Z$ , i.e.,  $\rho_i^z = \{z_{i,r} \in [l_r^z, u_r^z]\}_{r=1\dots k}$  (lower and upper bound are in the domain of  $z_{i,r}$ , extended with  $\pm\infty$ ). Then, by exploiting the linearity of  $\eta_i^b$ , these rules are converted into input space local oblique rules  $\tilde{\rho}_i^x = \{\sum_{j=1}^m W_{i,j,r}^b x_{i,j} \in [l_r^z, u_r^z]\}_{r=1\dots k}$ . Also, for more readability, we convert oblique rules into the axis-parallel format:  $\rho_i^x = \{x_{i,j} \in [l_{i,j}^x, u_{i,j}^x]\}_{j=1\dots m}$ . The upper and lower bounds for these rules satisfy the following constraints (details in Appendix C):

$$l_{i,j}^x - x_{i,j} = \max_r \frac{l_r^z - z_{i,r}}{W_{i,j,r}^b} \quad \text{and} \quad u_{i,j}^x - x_{i,j} = \min_r \frac{u_r^z - z_{i,r}}{W_{i,j,r}^b},$$

where the max/min operations ensure taking the most restrictive inequality among the  $k$  oblique latent conditions. Essentially, with ILLUME the global rules with bounds  $[l_r^z, u_r^z]$  are locally rescaled using the individual weights  $W_{i,j,r}^b$ . This rescaling makes the explanations more adaptive, tailoring them to the local contributions of each input feature. For instance, w.r.t. the previous example, we fit a surrogate tree  $g$  on the 2-dim

<sup>3</sup>This follows from applying the encoding  $z_{i,r} = \sum_{j=1}^m W_{i,j,r}^b x_{i,j}$  in the expression for  $g(\mathbf{z}_i)$ . For simplicity, we neglected the intercept  $\beta_0$  of the logistic classifier.

embedding  $Z$ , and obtain global latent rules  $\rho^z = \{-\infty \leq z_1 \leq \xi, \lambda \leq z_2 \leq +\infty\}$ . Due to the mapping linearity, we obtain the local axis-parallel rules as a function of the input features:  $\rho^x = \{x_{age} - \frac{\xi - z_1}{W_{age,1}^b} \leq x_{age} \leq x_{age} + \frac{\lambda - z_2}{W_{age,2}^b}, -\infty \leq x_{inc} \leq x_{inc} + \frac{\xi - z_1}{W_{inc,1}^b}, x_{edu} - \frac{\lambda - z_2}{W_{edu,2}^b} \leq x_{edu} \leq +\infty\}$ .

**Perfect Fidelity via Similarity Search.** Relying on surrogate logic, in ILLUME the explanations  $e_g(\mathbf{z}_i, \eta_i^b)$  are valid iff  $g(\eta_i^b(\mathbf{x}_i)) = b(\mathbf{x}_i)$ , i.e., when the surrogate correctly predicts the black-box. To ensure producing valid explanations for every instance, when  $g(\eta_i^b(\mathbf{x}_i)) \neq b(\mathbf{x}_i)$ , we perform a vector search to find in  $Z$  the nearest latent instance  $\mathbf{z}_j$  to  $\mathbf{z}_i$  s.t.  $g(\eta_j^b(\mathbf{x}_j)) = b(\mathbf{x}_j)$  and  $b(\mathbf{x}_i) = b(\mathbf{x}_j)$ , using its explanation  $e_g(\mathbf{z}_j, \eta_j^b)$  instead. This approach leverages ILLUME's design, which ensures that nearby points in latent space have similar transformations. Hence, explanations for these points remain closely aligned and reliable.

## IV. EXPERIMENTS

We run large-scale experiments to answer these research questions:

- **RQ1** - Is the latent space from ILLUME effective in preserving the original structure concerning both features and decisions?
- **RQ2** - Are black-box explanations generated with ILLUME accurate and aligned with true explanations?
- **RQ3** - Is ILLUME reliable enough to be trusted in the absence of ground-truth explanations?

### A. Experimental Setting

We summarize here the experimental setup<sup>4</sup>. For a detailed description of the datasets, model setups, hyper-parameter tuning, competitor details, and non-aggregated results, we refer the reader to Appendix A and E. Moreover, in Appendix B we show qualitative examples for the method's outputs and intermediate steps.

**Datasets.** We present our results on a variety of synthetic and real-world datasets used in prior works. In line with [79]–[81], for synthetic datasets, we utilize the SENECA framework for generating synthetic transparent classifiers, as proposed in [82]. Furthermore, we employ 18 real-world datasets from UCI Machine Learning Repository. As black-box classifiers, we consider the ensemble methods XGBoost (XGB) [83] and LightGBM (LGBM) [84], as they are among the most effective techniques for tabular data [85], [86].

**Model Setup.** We consider ILLUME-LR and ILLUME-DT, where as surrogate models  $g$  are used Logistic Regression to generate feature importance, and Decision Tree to derive rules. After hyper-parameter tuning on a validation set, we employ the best combination of regularizations, i.e., *soft-orthogonality*, and *non-collinearity*, abbreviated with *so*, and *co*. For sparsity, we test two opposite situations:  $\alpha = m$  (no sparsity), and  $\alpha = 2$  (max non-trivial sparsity). In each case, every single loss term is optimized with  $\lambda = 1$  or  $\lambda = 0$ . Also, in order to evaluate the impact of decision conditioning and consistency principles, we consider the UNConditioned (ILLUME-UC) and the UNStable

<sup>4</sup>Code and data repository: <https://github.com/simonepiaggessi/illumine>.

TABLE I: RQ1: Latent space quality metrics.

		ILL-UC	LIN-UC	PCA	ISOMAP	LLE	UMAP
<b>KNN Gain</b>	avg	<u>1.015</u>	1.002	<b>1.019</b>	.980	.943	.968
	rank	<b>2.14</b>	<u>2.69</u>	2.78	3.94	5.25	4.19
<b>Feature Pres.</b>	avg	<u>.937</u>	.933	<b>.986</b>	.819	.640	.739
	rank	<b>2.42</b>	2.44	<b>1.25</b>	3.94	5.94	5.00

**KNN gain**

LLE .943  
UMAP .968  
ISOMAP .980  
ILL-UC 1.015  
LIN-UC 1.002  
PCA 1.019

**Feature preservation**

LLE .640  
UMAP .739  
ISOMAP .819  
ILL-UC .937  
LIN-UC .933  
PCA .986

<b>LGBM,XGB</b>	<b>Decision Pres.</b>	
	avg	rank
ILL	<b>.687</b>	<b>1.31</b>
LIN	<u>.664</u>	<u>2.06</u>
ILL-UC	.629	3.14
LIN-UC	.626	3.50

**Decision preservation**

LIN-UC .626  
ILL-UC .629  
ILL .687  
LIN .664

(ILLUME-US) variations, setting to zero respectively  $\lambda^y$  and  $\lambda^{st}$ . Finally, we evaluate the impact of the local linearity assumption, by training a global linear encoding LIN where a single NN layer represents the function  $\eta^b$ , without non-linear activations.

**Competitors.** We compare ILLUME against latent embedding methods to evaluate the neighborhood structure preservation in the latent space: PCA [19], ISOMAP [49], LLE [50], (parametric-)UMAP [26]. We compare ILLUME with local explainers to evaluate the quality of explanations: LIME [7], SHAP [44], LORE [8], ANCHOR [87]. Finally, we compare ILLUME with global surrogate classifiers trained on the input space (INP-LR and INP-DT). For a fair comparison, we apply the latent search for maximizing surrogate fidelity also for LIN-LR and LIN-DT. Instead, for INP-LR and INP-DT we search the nearest neighbor in the input space. Each black-box, explainer or embedding is trained and evaluated on 80/20% splits of every dataset.

## B. Results and Discussion

In the following, we describe and discuss the main findings from the experiments. Within real-world data, tables display the average of best metrics across all datasets. Top methods are highlighted in bold for every metric, while the second-highest results are underlined. Additionally, we provide Critical Difference (CD) plots to compare statistically significant average ranks (with the null hypothesis rejected at  $p\text{-value} < .001$ ), determined using the non-parametric Friedman test, across multiple methods based on a single evaluation measure [88]. Two methods are tied if the null hypothesis that their performance is the same cannot be rejected using the Nemenyi test at 90% confidence level.

**RQ1 - Is the latent space from ILLUME effective in preserving the original structure concerning both features and decisions?** Using real-world datasets, we compared ILLUME against other dimensionality reduction frameworks to assess the quality of the latent spaces in preserving neighborhoods information.

TABLE II: RQ2: Explanation correctness for synthetic black-box. Prediction accuracy of surrogate models inside parentheses.

SENECA-RC $t + u$	Feature Importance Correctness				
	4+0	8+0	16+0	16+16	16+48
ILL-LR(co)	<u>.588</u> (87.6)	<u>.476</u> (79.9)	<b>.181</b> (78.6)	<b>.133</b> (77.5)	.077 (73.3)
ILL-LR-UC(co)	<b>.603</b> (87.2)	<b>.479</b> (79.6)	<u>.170</u> (79.1)	<u>.124</u> (77.0)	<b>.085</b> (72.7)
ILL-LR-US(co)	.503 (85.1)	.393 (77.6)	<b>.181</b> (78.8)	<u>.110</u> (73.1)	<u>.081</u> (72.7)
LIN-LR(co)	.289 (79.1)	.226 (73.7)	.163 (77.3)	.094 (74.8)	.022 (66.0)
INP-LR	.275 (78.3)	.217 (73.2)	.107 (75.3)	.092 (74.9)	<u>.080</u> (75.8)
LIME	.420	.267	.102	.076	.054
SHAP	.303	.350	.030	.031	.030

SENECA-RB $t + u$	Decision Rule Correctness				
	4+0	8+0	16+0	16+16	16+48
ILL-DT(so, $\alpha=2$ )	.531 (71.6)	.339 (74.4)	<u>.240</u> (73.3)	<u>.200</u> (71.9)	<u>.166</u> (70.3)
ILL-DT-UC(so, $\alpha=2$ )	.523 (72.1)	.318 (73.9)	.209 (71.3)	.165 (69.3)	.128 (66.6)
ILL-DT-US(so, $\alpha=2$ )	.504 (70.9)	.308 (74.4)	.218 (73.1)	.199 (73.1)	.143 (68.8)
LIN-DT(so, $\alpha=2$ )	<u>.545</u> (71.2)	.344 (74.8)	.226 (73.8)	.165 (71.3)	.116 (65.4)
INP-DT	<u>.545</u> (70.5)	<b>.356</b> (72.8)	<b>.266</b> (71.2)	<b>.244</b> (69.8)	<b>.227</b> (69.6)
LORE	<b>.557</b>	<u>.346</u>	.202	.150	.123
ANCHOR	.402	.326	.204	.156	.139

In Table I, is reported the *KNN Gain* [34], defined as the ratio of a KNN classifier's accuracy in the low-dimensional space to its accuracy in the original one,  $\frac{acc_{KNN}(Z)}{acc_{KNN}(X)}$ . This evaluation is based on the principle of homophily, assuming that instances within the same ground-truth class are closely clustered together, an effective latent encoding should reinforce these similarities, enabling gains when the latent configuration of instances is better organized. At this stage we remove the effects of label conditioning by studying ILLUME-UC and its variants. Moreover, we did not observe significant improvement with regularizations. Our analysis reveals that ILLUME-UC ranks as the top-performing method, while its average performance is comparable to that of PCA.

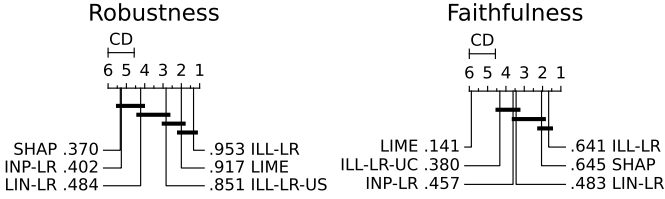
In Table I we also assess whether the global arrangement of the neighborhoods is preserved in terms of *Feature Preservation* and *Decision Preservation* calculated with *triplet accuracy*. The *triplet accuracy* [47] measures the percentage of triplets for which the relative ordering of pairwise distances remains consistent between the original and projected spaces. Thus, *Feature Preservation* compares the pairwise latent distance orderings  $\|z_i - z_j\|_2$  with the original feature-based distances  $\|x_i - x_j\|_2$ , while the *Decision Preservation* compares  $\|z_i - z_j\|_2$  with relative distances of black-box decisions  $\|b(x)_i - b(x)_j\|_2$ . In line with the *KNN Gain* results, when comparing feature preservation across dimensionality reduction methods, ILLUME-UC ranks second only to PCA and performs similarly to LIN-UC. On the other hand, in terms of decision preservation, label conditioning in ILLUME is determinant for significantly enhancing triplet accuracy, even outperforming LIN. Appendix E reports surrogate classification accuracies with decision conditioning, showing similar findings. These results highlight ILLUME's ability to capture black-box decision logic and feature proximity in latent representations.

**RQ2 - Are black-box explanations generated with ILLUME accurate and aligned with true explanations?** We employed SENECA-RB and SENECA-RC [82] to study the



TABLE III: RQ3: Robustness and faithfulness for feature importance explanations.

<b>Robustness</b>	ILL-LR (co)	ILL-LR-US (co)	LIN-LR (co)	INP-LR	LIME	SHAP
avg	<b>.953</b>	.851	.484	.402	<u>.917</u>	.370
rank	<b>1.33</b>	2.83	4.22	5.28	<u>2.00</u>	5.33
<b>Faithfulness</b>	ILL-LR (.)	ILL-LR-UC (.)	LIN-LR (so, $\alpha=2$ )	INP-LR	LIME	SHAP
avg	<u>.641</u>	.380	.483	.457	.141	<b>.645</b>
rank	<b>1.67</b>	4.33	3.44	3.61	5.88	<u>2.06</u>



*explanation correctness* of local model-agnostic explainers on tabular data. By exploiting synthetic transparent classifiers and treating them as black-boxes, we can directly compare the explanations provided by an explainer with the ground-truth decision logic of the synthetic black-box<sup>5</sup>. We evaluate the correctness of local explanations by measuring the closeness between the extracted explanations  $\epsilon$  and the ground-truth  $\hat{\epsilon}$  provided by the synthetic classifiers of SENECA. Following [79], [82], for feature importance we measure the proximity of two explanations with the *cosine similarity score* of attribution vectors:  $cs\text{-}score(\psi, \hat{\psi}) = \frac{\psi \cdot \hat{\psi}}{\|\psi\| \|\hat{\psi}\|}$ . Besides, for decision rules we measure the similarity of the bounded regions of the instance space described by two rules, calculating the closeness between upper and lower bounds when both are different from  $\pm\infty$  (*complete rule score*<sup>6</sup>):  $cplt\text{-}score(\rho, \hat{\rho}) = \frac{1}{N_{\infty}} \left( \sum_{l \neq \pm\infty} \frac{1}{1+|\rho_l - \hat{\rho}_l|^2} + \sum_{u \neq \pm\infty} \frac{1}{1+|\rho_u - \hat{\rho}_u|^2} \right)$ .

Table II reports explanation correctness on synthetic data from SENECA-RC and SENECA-RB, using the best regularizer for ILLUME and LIN. Explanation metrics generally decreases with noisy input dimensions denoted with  $u$  (while  $t$  refers to informative dimensions). ILLUME-LR consistently outperforms LIN-LR and INP-LR in surrogate performance. For feature importance explanations, ILL-LR and its variants (ILL-LR-UC, ILL-LR-US) significantly surpass competitors, with label conditioning and consistency having minimal impact. For decision rule explanations, ILL-DT ranks second-best for input dimensions  $\geq 16$ , always outperforming ILL-DT-UC/ILL-DT-US and surpassing LIN-DT for dimensions  $\geq 8$ . INP-DT performs best, as expected, since SENECA-RB is based on decision trees trained in the input space, aligning its structure with the ground-truth logic. Appendix E provides further tests on regularization effects.

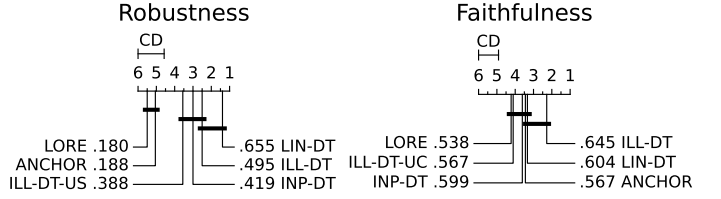
### RQ3 - Is ILLUME reliable enough to be trusted in

<sup>5</sup>Please refer to [82] for the definitions of ground-truth explanations.

<sup>6</sup>When an infinite lower/upper bound is compared with a finite one, the condition counts zero because  $\frac{1}{1 \pm \infty} = 0$ . In [82], the author uses a simpler metric based on binary thresholding  $|\rho_l - \hat{\rho}_l|$  and  $|\rho_u - \hat{\rho}_u|$ . Our proposed metric captures differences in a continuous spectrum, spanning between 0 and 1 as well.

TABLE IV: RQ3: Robustness and faithfulness for rule-based explanations.

<b>Robustness</b>	ILL-DT (so, $\alpha=2$ )	ILL-DT-US (so, $\alpha=2$ )	LIN-DT (so, $\alpha=2$ )	INP-DT	LORE	ANCHOR
avg	<u>.495</u>	.388	<b>.655</b>	.419	.180	.188
rank	<u>2.50</u>	3.56	<b>1.39</b>	3.00	5.50	5.06
<b>Faithfulness</b>	ILL-DT (so, $\alpha=2$ )	ILL-DT-UC (so, $\alpha=2$ )	LIN-DT (so, $\alpha=2$ )	INP-DT	LORE	ANCHOR
avg	<b>.645</b>	<u>.567</u>	.604	.599	.538	<u>.567</u>
rank	<b>2.26</b>	4.11	<u>3.33</u>	3.61	4.22	3.44



**the absence of ground-truth explanations?** Resorting real-world datasets, we compared ILLUME against local model-agnostic explainers to assess the trustworthiness of the resulting explanations. Since ground-truth for individual explanations is unavailable in real-world data [82], we focus on other criteria that are critical for explanations' evaluation, i.e., (i) their sensitivity to feature modifications (*Robustness*) [12], [89], and (ii) their ability to accurately reflect the reasoning of the black-box model (*Faithfulness* or fidelity) [90], [91].

In line with [89], we evaluate robustness for each instance as the maximum change in the explanation with small input perturbations. For each test instance  $\mathbf{x}_i$ , we compute the average maximum sensitivity over multiple nearest neighborhoods ( $K_{max} = 20$ )  $\frac{1}{K_{max}} \sum_{K=1}^{K_{max}} \max_{j \in \mathcal{N}_K(i)} d_{\mathcal{E}}(i, j)$ , where  $\mathcal{N}_K(i)$  denotes the set of  $K$  nearest neighbors of  $\mathbf{x}_i$  with same predicted black-box label, and  $d_{\mathcal{E}}(i, j)$  is a suitable pairwise explanations distance. In line with [91], we evaluate fidelity by assessing whether similar black-box predictions result in similar explanations. Thus, faithfulness is evaluated by measuring the rank correlation between the pairwise distances of explanations,  $\{d_{\mathcal{E}}(i, j)\}_{i < j}$ , and the corresponding pairwise differences in black-box predictions,  $\{\|b(\mathbf{x}_i) - b(\mathbf{x}_j)\|_2\}_{i < j}$ . Similarly to SENECA, we use the similarity metrics *cs-score* and *cplt-score* instead of distance metrics to evaluate explanation proximity. For robustness, we select the most dissimilar explanations within each neighborhood. In Appendix E, we also report interesting findings based on a global definition of robustness.

Tables III and IV present the results, with CD plots summarizing overall performance across datasets and black-boxes. Table III reports metrics for importance-based explainers, where ILLUME-LR excels in robustness, followed by LIME, while methods without stability optimization underperform. For faithfulness, ILLUME-LR and SHAP lead, whereas removing decision conditioning reduces effectiveness. Table IV evaluates rule-based explainers, showing ILLUME-DT and LIN-DT as the most robust, with LIN-DT ranking highest, suggesting globally linear encodings enhance stability. Like ILLUME-LR-US, ILLUME-DT-US shows a notable drop.



## V. CONCLUSIONS

We have introduced ILLUME, a generative framework for local explanations compatible with any interpretable surrogate model. Unlike traditional surrogate-based explainers, which often fail to satisfy desirable explanation properties, ILLUME represents a paradigm shift by combining global reasoning capabilities of interpretable surrogates with local linear encodings of input features. Through extensive experiments on tabular datasets, we have empirically demonstrated that ILLUME produces explanations that are accurate, robust, and faithful, achieving performance comparable to or surpassing state-of-the-art attribution-based and rule-based explainers in most cases.

As future work, ILLUME can be extended to end-to-end training a meta-surrogate model, where, like self-interpretable models [92], explainability is built-in architecturally and enforced through task-specific constraints. Additionally, we aim to explore generalizations for constructing interpretable-by-design classifiers rather than relying on post-hoc explanations as presented in this study. Moreover, by leveraging recent advances in tabular foundation models [93], the presented methodology can be further generalized to develop cross-dataset explanation inference frameworks.

## ACKNOWLEDGMENTS

This work has been partially supported by the European Community Horizon 2020 programme under the funding scheme ERC-2018-ADG G.A. 834756 *XAI: Science and technology for the eXplanation of AI decision making* (<https://xai-project.eu/index.html>), and the NextGenerationEU programme under the funding schemes: PNRR-PE-AI (M4C2, investment 1.3, line on AI) *FAIR* (Future Artificial Intelligence Research), and “*SoBigData.it* - Strengthening the Italian RI for Social Mining and Big Data Analytics” - Prot. IR0000013, and by the Italian Project Fondo Italiano per la Scienza FIS00001966 MIMOSA.

## REFERENCES

- [1] F. Bodria, F. Giannotti, R. Guidotti, F. Naretto, D. Pedreschi, and S. Rinzivillo, “Benchmarking and survey of explanation methods for black box models,” *Data Min. Knowl. Discov.*, vol. 37, no. 5, pp. 1719–1778, 2023.
- [2] N. Burkart and M. F. Huber, “A survey on the explainability of supervised machine learning,” *J. Artif. Intell. Res.*, vol. 70, pp. 245–317, 2021.
- [3] R. Guidotti, “Counterfactual explanations and how to find them: literature review and benchmarking,” *Data Min. Knowl. Discov.*, vol. 38, no. 5, pp. 2770–2824, 2024.
- [4] J. Herbringer, S. Dandl, F. K. Ewald, S. Loibl, and G. Casalicchio, “Leveraging model-based trees as interpretable surrogate models for model distillation,” in *ECAI Workshops (1)*, ser. Communications in Computer and Information Science, vol. 1947. Springer, 2023, pp. 232–249.
- [5] N. Frosst and G. E. Hinton, “Distilling a neural network into a soft decision tree,” in *CEx@AI\*IA*, ser. CEUR Workshop Proceedings, vol. 2071. CEUR-WS.org, 2017.
- [6] M. W. Craven and J. W. Shavlik, “Extracting tree-structured representations of trained networks,” in *NIPS*. MIT Press, 1995, pp. 24–30.
- [7] M. T. Ribeiro, S. Singh, and C. Guestrin, ““why should I trust you?”: Explaining the predictions of any classifier,” in *KDD*. ACM, 2016.
- [8] R. Guidotti, A. Monreale, S. Ruggieri, F. Naretto, F. Turini, D. Pedreschi, and F. Giannotti, “Stable and actionable explanations of black-box models through factual and counterfactual rules,” *Data Min. Knowl. Discov.*, vol. 38, no. 5, pp. 2825–2862, 2024.
- [9] E. Doumard, J. Aligon, E. Escriva, J. Excoffier, P. Monsarrat, and C. Soulé-Dupuy, “A quantitative approach for the comparison of additive local explanation methods,” *Inf. Syst.*, vol. 114, p. 102162, 2023.
- [10] Y. Zhou, S. Booth, M. T. Ribeiro, and J. Shah, “Do feature attribution methods correctly attribute features?” in *AAAI*. AAAI Press, 2022, pp. 9623–9633.
- [11] X. Huang and J. Marques-Silva, “The inadequacy of shapley values for explainability,” *CoRR*, vol. abs/2302.08160, 2023.
- [12] D. Alvarez-Melis and T. S. Jaakkola, “On the robustness of interpretability methods,” *CoRR*, vol. abs/1806.08049, 2018.
- [13] D. Garreau and U. von Luxburg, “Explaining the explainer: A first theoretical analysis of LIME,” in *AISTATS*, ser. Proceedings of Machine Learning Research, vol. 108. PMLR, 2020, pp. 1287–1296.
- [14] N. Bansal, C. Agarwal, and A. Nguyen, “SAM: the sensitivity of attribution methods to hyperparameters,” in *CVPR Workshops*. Computer Vision Foundation / IEEE, 2020, pp. 11–21.
- [15] Y. Zhang, K. Song, Y. Sun, S. Tan, and M. Udell, ““why should you trust my explanation?” understanding uncertainty in lime explanations,” *arXiv preprint arXiv:1904.12991*, 2019.
- [16] S. M. Lundberg, G. G. Erion, H. Chen, A. J. DeGrave, J. M. Prutkin, B. Nair, R. Katz, J. Himmelfarb, N. Bansal, and S. Lee, “From local explanations to global understanding with explainable AI for trees,” *Nat. Mach. Intell.*, vol. 2, no. 1, pp. 56–67, 2020.
- [17] K. Aas, M. Jullum, and A. Løland, “Explaining individual predictions when features are dependent: More accurate approximations to shapley values,” *Artif. Intell.*, vol. 298, p. 103502, 2021.
- [18] P. Kindermans, S. Hooker, J. Adebayo, M. Alber, K. T. Schütt, S. Dähne, D. Erhan, and B. Kim, “The (un)reliability of saliency methods,” in *Explainable AI*, ser. Lecture Notes in Computer Science. Springer, 2019, vol. 11700, pp. 267–280.
- [19] H. Abdi and L. J. Williams, “Principal component analysis,” *Wiley interdisciplinary reviews: computational statistics*, vol. 2, no. 4, pp. 433–459, 2010.
- [20] A. Dhurandhar, K. N. Ramamurthy, and K. Shanmugam, “Is this the right neighborhood? accurate and query efficient model agnostic explanations,” in *NeurIPS*, 2022.
- [21] T. Laugel, X. Renard, M. Lesot, C. Marsala, and M. Detryniecki, “Defining locality for surrogates in post-hoc interpretability,” *CoRR*, vol. abs/1806.07498, 2018.
- [22] Y. Bengio, A. C. Courville, and P. Vincent, “Representation learning: A review and new perspectives,” *IEEE Trans. Pattern Anal. Mach. Intell.*, vol. 35, no. 8, pp. 1798–1828, 2013.
- [23] D. Danks and C. Yau, “Basisdevae: Interpretable simultaneous dimensionality reduction and feature-level clustering with derivative-based variational autoencoders,” in *ICML*, ser. Proceedings of Machine Learning Research, vol. 139. PMLR, 2021, pp. 2410–2420.
- [24] Y. Pu, Z. Gan, R. Henao, X. Yuan, C. Li, A. Stevens, and L. Carin, “Variational autoencoder for deep learning of images, labels and captions,” in *NIPS*, 2016, pp. 2352–2360.
- [25] G. Lee, D. Alvarez-Melis, and T. S. Jaakkola, “Towards robust, locally linear deep networks,” in *ICLR (Poster)*. OpenReview.net, 2019.
- [26] T. Sainburg, L. McInnes, and T. Q. Gentner, “Parametric UMAP embeddings for representation and semisupervised learning,” *Neural Comput.*, vol. 33, no. 11, pp. 2881–2907, 2021.
- [27] L. Van der Maaten and G. Hinton, “Visualizing data using t-sne,” *Journal of machine learning research*, vol. 9, no. 11, 2008.
- [28] P. W. Koh, T. Nguyen, Y. S. Tang, S. Mussmann, E. Pierson, B. Kim, and P. Liang, “Concept bottleneck models,” in *ICML*, ser. Proceedings of Machine Learning Research, vol. 119. PMLR, 2020, pp. 5338–5348.
- [29] A. S. Zharmagambetov and M. Á. Carreira-Perpiñán, “Learning interpretable, tree-based projection mappings for nonlinear embeddings,” in *AISTATS*, ser. Proceedings of Machine Learning Research, vol. 151. PMLR, 2022, pp. 9550–9570.
- [30] E. Marconato, A. Passerini, and S. Teso, “Glancenets: Interpretable, leak-proof concept-based models,” in *NeurIPS*, 2022.
- [31] M. E. Zarlenga, P. Barbiero, G. Ciravegna, G. Marra, F. Giannini, M. Diligenti, Z. Shams, F. Precioso, S. Melacci, A. Weller, P. Lió, and M. Jamnik, “Concept embedding models: Beyond the accuracy-explainability trade-off,” in *NeurIPS*, 2022.
- [32] S. Piaggese, F. Bodria, R. Guidotti, F. Giannotti, and D. Pedreschi, “Counterfactual and prototypical explanations for tabular data via interpretable latent space,” *IEEE Access*, vol. 12, pp. 168 983–169 000, 2024.
- [33] D. Kunin, J. M. Bloom, A. Goeva, and C. Seed, “Loss landscapes of regularized linear autoencoders,” in *ICML*, ser. Proceedings of Machine Learning Research, vol. 97. PMLR, 2019, pp. 3560–3569.
- [34] F. Bodria, R. Guidotti, F. Giannotti, and D. Pedreschi, “Transparent latent space counterfactual explanations for tabular data,” in *DSAA*. IEEE, 2022, pp. 1–10.

- [35] Y. Takai, A. Sannai, and M. Cordonnier, "On the number of linear functions composing deep neural network: Towards a refined definition of neural networks complexity," in *AISTATS*, ser. Proceedings of Machine Learning Research, vol. 130. PMLR, 2021, pp. 3799–3807.
- [36] R. Agarwal, L. Melnick, N. Frosst, X. Zhang, B. J. Lengerich, R. Caruana, and G. E. Hinton, "Neural additive models: Interpretable machine learning with neural nets," in *NeurIPS*, 2021, pp. 4699–4711.
- [37] Y. Lou, R. Caruana, J. Gehrke, and G. Hooker, "Accurate intelligible models with pairwise interactions," in *KDD*. ACM, 2013, pp. 623–631.
- [38] A. Cremades, S. Hoyas, and R. Vinuesa, "Additive-feature-attribution methods: a review on explainable artificial intelligence for fluid dynamics and heat transfer," *CoRR*, vol. abs/2409.11992, 2024.
- [39] C. Molnar, *Interpretable Machine Learning*, 2020, <https://christophm.github.io/interpretable-ml-book/>.
- [40] W. Samek and K. Müller, "Towards explainable artificial intelligence," in *Explainable AI*, ser. Lecture Notes in Computer Science. Springer, 2019, vol. 11700, pp. 5–22.
- [41] Z. Tan, Y. Tian, and J. Li, "GLIME: general, stable and local LIME explanation," in *NeurIPS*, 2023.
- [42] S. M. Shankaranarayana and D. Runje, "ALIME: autoencoder based approach for local interpretability," in *IDEAL (I)*, ser. Lecture Notes in Computer Science, vol. 11871. Springer, 2019, pp. 454–463.
- [43] R. Guidotti, A. Monreale, F. Giannotti, D. Pedreschi, S. Ruggieri, and F. Turini, "Factual and counterfactual explanations for black box decision making," *IEEE Intell. Syst.*, vol. 34, no. 6, pp. 14–23, 2019.
- [44] S. M. Lundberg and S. Lee, "A unified approach to interpreting model predictions," in *NIPS*, 2017, pp. 4765–4774.
- [45] M. Setzu, R. Guidotti, A. Monreale, F. Turini, D. Pedreschi, and F. Giannotti, "Glocalx - from local to global explanations of black box AI models," *Artif. Intell.*, vol. 294, p. 103457, 2021.
- [46] A. Björklund, J. Mäkelä, and K. Puolamäki, "SLISEMAP: supervised dimensionality reduction through local explanations," *Mach. Learn.*, vol. 112, no. 1, pp. 1–43, 2023.
- [47] Y. Wang *et al.*, "Understanding how dimension reduction tools work: An empirical approach to deciphering t-sne, umap, trimap, and pacmap for data visualization," *J. Mach. Learn. Res.*, vol. 22, pp. 201:1–201:73, 2021.
- [48] N. Saeed, H. Nam, M. I. U. Haq, and D. M. S. Bhatti, "A survey on multidimensional scaling," *ACM Comput. Surv.*, vol. 51, no. 3, pp. 47:1–47:25, 2018.
- [49] J. B. Tenenbaum, V. d. Silva, and J. C. Langford, "A global geometric framework for nonlinear dimensionality reduction," *science*, vol. 290, no. 5500, pp. 2319–2323, 2000.
- [50] S. T. Roweis and L. K. Saul, "Nonlinear dimensionality reduction by locally linear embedding," *science*, vol. 290, no. 5500, pp. 2323–2326, 2000.
- [51] L. McInnes and J. Healy, "UMAP: uniform manifold approximation and projection for dimension reduction," *CoRR*, vol. abs/1802.03426, 2018.
- [52] L. K. Senel, I. Utlu, V. Yücesoy, A. Koç, and T. Çukur, "Semantic structure and interpretability of word embeddings," *IEEE ACM Trans. Audio Speech Lang. Process.*, vol. 26, no. 10, pp. 1769–1779, 2018.
- [53] A. Simhi and S. Markovitch, "Interpreting embedding spaces by conceptualization," in *EMNLP*. Association for Computational Linguistics, 2023, pp. 1704–1719.
- [54] R. Plesh, J. Krizaj, K. Bahmani, M. Banavar, V. Struc, and S. Schuckers, "Discovering interpretable feature directions in the embedding space of face recognition models," in *IJCB*. IEEE, 2024, pp. 1–10.
- [55] A. Subramanian, D. Pruthi, H. Jhamtani, T. Berg-Kirkpatrick, and E. H. Hovy, "SPINE: sparse interpretable neural embeddings," in *AAAI*. AAAI Press, 2018, pp. 4921–4928.
- [56] V. Sitzmann, J. N. P. Martel, A. W. Bergman, D. B. Lindell, and G. Wetzstein, "Implicit neural representations with periodic activation functions," in *NeurIPS*, 2020.
- [57] L. Xu, M. Skoularidou, A. Cuesta-Infante, and K. Veeramachaneni, "Modeling tabular data using conditional GAN," in *NeurIPS*, 2019, pp. 7333–7343.
- [58] H. GM, M. K. Gourisaria, M. Pandey, and S. S. Rautaray, "A comprehensive survey and analysis of generative models in machine learning," *Comput. Sci. Rev.*, vol. 38, p. 100285, 2020.
- [59] X. Chen, M. Ding, X. Wang, Y. Xin, S. Mo, Y. Wang, S. Han, P. Luo, G. Zeng, and J. Wang, "Context autoencoder for self-supervised representation learning," *Int. J. Comput. Vis.*, vol. 132, no. 1, pp. 208–223, 2024.
- [60] L. Le, A. Patterson, and M. White, "Supervised autoencoders: Improving generalization performance with unsupervised regularizers," in *NeurIPS*, 2018, pp. 107–117.
- [61] C. Conwell, D. Mayo, A. Barbu, M. A. Buice, G. Alvarez, and B. Katz, "Neural regression, representational similarity, model zoology & neural taskonomy at scale in rodent visual cortex," in *NeurIPS*, 2021, pp. 5590–5607.
- [62] J. Crabbé, Z. Qian, F. Imrie, and M. van der Schaar, "Explaining latent representations with a corpus of examples," in *NeurIPS*, 2021, pp. 12 154–12 166.
- [63] R. Guidotti, A. Monreale, S. Matwin, and D. Pedreschi, "Black box explanation by learning image exemplars in the latent feature space," in *ECML/PKDD (I)*, ser. Lecture Notes in Computer Science, vol. 11906. Springer, 2019, pp. 189–205.
- [64] F. Spinnato, R. Guidotti, A. Monreale, M. Nanni, D. Pedreschi, and F. Giannotti, "Understanding any time series classifier with a subsequence-based explainer," *ACM Trans. Knowl. Discov. Data*, vol. 18, no. 2, pp. 36:1–36:34, 2024.
- [65] R. Crupi, A. Castelnovo, D. Regoli, and B. S. M. González, "Counterfactual explanations as interventions in latent space," *Data Min. Knowl. Discov.*, vol. 38, no. 5, pp. 2733–2769, 2024.
- [66] Z. Wang, I. Samsten, R. Mochaourab, and P. Papapetrou, "Learning time series counterfactuals via latent space representations," in *DS*, ser. Lecture Notes in Computer Science, vol. 12986. Springer, 2021, pp. 369–384.
- [67] V. Guyomard, F. Fessant, T. Guyet, T. Bouadi, and A. Termier, "Vcnet: A self-explaining model for realistic counterfactual generation," in *ECML/PKDD (I)*, ser. Lecture Notes in Computer Science, vol. 13713. Springer, 2022, pp. 437–453.
- [68] D. Alvarez-Melis and T. S. Jaakkola, "Towards robust interpretability with self-explaining neural networks," pp. 7786–7795, 2018.
- [69] S. Lee, X. Wang, S. Han, X. Yi, X. Xie, and M. Cha, "Self-explaining deep models with logic rule reasoning," in *NeurIPS*, 2022.
- [70] W. Guo, S. Huang, Y. Tao, X. Xing, and L. Lin, "Explaining deep learning models—a bayesian non-parametric approach," in *Advances in neural information processing systems*, vol. 31, 2018.
- [71] W. Harvey, S. Naderiparizi, and F. Wood, "Conditional image generation by conditioning variational auto-encoders," in *ICLR*. OpenReview.net, 2022.
- [72] K. Sokol and P. A. Flach, "Interpretable representations in explainable AI: from theory to practice," *Data Min. Knowl. Discov.*, vol. 38, no. 5, pp. 3102–3140, 2024.
- [73] S. Yang, S. Huang, W. Zou, J. Zhang, X. Dai, and J. Chen, "Local interpretation of transformer based on linear decomposition," in *ACL (I)*. Association for Computational Linguistics, 2023, pp. 10 270–10 287.
- [74] L. Gao, T. D. la Tour, H. Tillman, G. Goh, R. Troll, A. Radford, I. Sutskever, J. Leike, and J. Wu, "Scaling and evaluating sparse autoencoders," *CoRR*, vol. abs/2406.04093, 2024.
- [75] A. Makhzani and B. J. Frey, "k-sparse autoencoders," in *ICLR (Poster)*, 2014.
- [76] E. M. Massart, "Orthogonal regularizers in deep learning: how to handle rectangular matrices?" in *ICPR*. IEEE, 2022, pp. 1294–1299.
- [77] M. Blondel, O. Teboul, Q. Berthet, and J. Djolonga, "Fast differentiable sorting and ranking," in *ICML*, ser. Proceedings of Machine Learning Research, vol. 119. PMLR, 2020, pp. 950–959.
- [78] D. P. Kingma and J. Ba, "Adam: A method for stochastic optimization," in *ICLR (Poster)*, 2015, pp. 1–9.
- [79] A. H. A. Rahnama, "The blame problem in evaluating local explanations and how to tackle it," in *ECAI Workshops (I)*, ser. Communications in Computer and Information Science, vol. 1947. Springer, 2023, pp. 66–86.
- [80] I. Mollas, N. Bassiliades, and G. Tsoumakas, "Truthful meta-explanations for local interpretability of machine learning models," *Appl. Intell.*, vol. 53, no. 22, pp. 26 927–26 948, 2023.
- [81] T. T. Nguyen, T. L. Nguyen, and G. Ifrim, "Robust explainer recommendation for time series classification," *Data Min. Knowl. Discov.*, vol. 38, no. 6, pp. 3372–3413, 2024.
- [82] R. Guidotti, "Evaluating local explanation methods on ground truth," *Artif. Intell.*, vol. 291, p. 103428, 2021.
- [83] T. Chen and C. Guestrin, "Xgboost: A scalable tree boosting system," in *KDD*. ACM, 2016, pp. 785–794.
- [84] G. Ke, Q. Meng, T. Finley, T. Wang, W. Chen, W. Ma, Q. Ye, and T. Liu, "Lightgbm: A highly efficient gradient boosting decision tree," in *NIPS*, 2017, pp. 3146–3154.
- [85] L. Grinsztajn, E. Oyallon, and G. Varoquaux, "Why do tree-based models still outperform deep learning on typical tabular data?" in *NeurIPS*, 2022.
- [86] R. Shwartz-Ziv and A. Armon, "Tabular data: Deep learning is not all you need," *Inf. Fusion*, vol. 81, pp. 84–90, 2022.

- [87] M. T. Ribeiro, S. Singh, and C. Guestrin, “Anchors: High-precision model-agnostic explanations,” in *AAAI*. AAAI Press, 2018, pp. 1527–1535.
- [88] J. Demsar, “Statistical comparisons of classifiers over multiple data sets,” *J. Mach. Learn. Res.*, vol. 7, pp. 1–30, 2006.
- [89] C. Yeh, C. Hsieh, A. S. Suggala, D. I. Inouye, and P. Ravikumar, “On the (in)fidelity and sensitivity of explanations,” pp. 10 965–10 976, 2019.
- [90] U. Bhatt, A. Weller, and J. M. F. Moura, “Evaluating and aggregating feature-based model explanations,” in *IJCAI*. ijcai.org, 2020, pp. 3016–3022.
- [91] S. Dasgupta, N. Frost, and M. Moshkovitz, “Framework for evaluating faithfulness of local explanations,” in *ICML*, ser. Proceedings of Machine Learning Research, vol. 162. PMLR, 2022, pp. 4794–4815.
- [92] Y. Ji, Y. Sun, Y. Zhang, Z. Wang, Y. Zhuang, Z. Gong, D. Shen, C. Qin, H. Zhu, and H. Xiong, “A comprehensive survey on self-interpretable neural networks,” *CoRR*, vol. abs/2501.15638, 2025.
- [93] B. van Breugel and M. van der Schaar, “Position: Why tabular foundation models should be a research priority,” in *ICML*. OpenReview.net, 2024.
- [94] B. McCane and M. H. Albert, “Distance functions for categorical and mixed variables,” *Pattern Recognit. Lett.*, vol. 29, no. 7, pp. 986–993, 2008.
- [95] A. H. Foss, M. Markatou, and B. Ray, “Distance metrics and clustering methods for mixed-type data,” *International Statistical Review*, vol. 87, no. 1, pp. 80–109, 2019.
- [96] A. H. A. Rahnama, J. Bütepage, P. Geurts, and H. Boström, “Can local explanation techniques explain linear additive models?” *Data Min. Knowl. Discov.*, vol. 38, no. 1, pp. 237–280, 2024.

TABLE A1: Real-world data characteristics and black-box performances. In order: number of instances  $n$ , number of total features  $m$ , categorical features  $h$ , number of classes  $c$ , majority and minority class percentages, macro-F1 classification scores for XGB and LGBM.

Dataset	$n$	$m$	$h$	$c$	maj(%)	min(%)	XGB	LGBM
aids	2,139	36	26	2	.756	.244	.893	.895
austr	690	46	40	2	.555	.445	.912	.905
bank	4,119	63	53	2	.891	.109	.775	.786
breast	569	30	0	2	.627	.373	.972	.991
churn	3,333	71	55	2	.855	.145	.946	.930
compas	7,214	20	13	2	.723	.277	.714	.711
ctg	2,126	56	33	3	.778	.083	.979	.982
diabts	768	8	0	2	.651	.349	.803	.805
ecoli	336	7	0	8	.426	.006	.859	.876
fico	10,459	23	0	2	.522	.478	.733	.733
german	1,000	61	54	2	.700	.300	.706	.706
home	492	7	0	2	.545	.455	.949	.959
ionos	351	34	0	2	.641	.359	.938	.953
sonar	208	60	0	2	.534	.466	.881	.881
spam	4,601	57	0	2	.606	.394	.959	.960
titnc	891	9	5	2	.616	.384	.841	.830
wine	6,497	11	0	7	.437	.001	.426	.433
yeast	1,484	8	0	10	.312	.003	.592	.527

## APPENDIX

### A. Detailed Experimental Settings

**Datasets.** We implement synthetic classifiers from SENECA framework [82] by varying the dimensions of the synthetic instances. In particular, we adjust the number of informative features ( $t$ ), and uninformative features ( $u$ ). The total number of features,  $m = t + u$ , is set in the list  $\{4, 8, 16, 32, 64\}$  and, for a fixed  $t + u$ , we define  $t = \min\{16, t + u\}$ . For each dataset dimension, we generate five rule-based classifiers and five linear classifiers. Hence, we explain 2,048 instances for each of them. Besides synthetic data, we employ 18 real-world datasets from UCI ML Repository<sup>7</sup>. In every dataset, we apply standard scaling, with zero mean and unitary variance to continuous features, and one-hot encoding to categorical features. Details for dataset characteristics after preprocessing are reported in Table A1.

**Black-boxes.** As black-box classifiers, we consider the ensemble methods XGBoost (XGB) [83] and LightGBM (LGBM) [84], because they are among the most effective techniques for tabular data, even outperforming deep learning models [85], [86]. Anyway, there is no specified limitation in using other black-boxes, such as NNs or SVMs. Each black-box is trained using 80% of the dataset, with the remaining 20% reserved for testing and evaluation. The black-box models are trained on each dataset’s classification tasks, whether binary or multi-class. For binary datasets, each explanation method is asked to generate explanations for the class 1. For multi-class datasets, each explanation method is asked to generate explanations for the majority class.

**Experimental setup for ILLUME.** The function  $f$  is implemented as a 3-layer fully-connected neural network. We did not tune the architecture with respect to the best number of layers and/or hidden sizes. Meta-encoder training is done

with Adam optimizer, fixing learning rate to  $10^{-3}$ , with early stopping technique to prevent overfitting. To compute the loss functions, for the latent space vectors we use the cosine distance<sup>8</sup>,  $d_{\mathcal{Z}}(i, j) = d_{\cos}(\mathbf{z}_i, \mathbf{z}_j)$ . In line with [8], [94], [95], we divide the input distance into contributions from continuous and categorical (one-hot encoded) features. Assuming  $h$  categorical features after one-hot encoding, we express the input distance<sup>9</sup> as  $d_{\mathcal{X}}(i, j) = \frac{h-m}{m}d_{\cos}(\mathbf{x}_i^{\text{con}}, \mathbf{x}_j^{\text{con}}) + \frac{h}{m}d_{hmm}(\mathbf{x}_i^{\text{cat}}, \mathbf{x}_j^{\text{cat}})$ . For the black-box score vectors, we employ cosine distance as well. For latent space transformation matrices, we consider the average per-column cosine distance  $d_{\mathcal{W}}(i, j) = \frac{1}{k} \sum_r d_{\cos}(W_{i,:r}^b, W_{j,:r}^b)$ . All the encodings are tested tuning the latent space dimension as hyperparameter from the list  $\{2, 4, 8, 16, 32\}$ .

**Experimental Setup for Dimensionality Reduction.** We compare ILLUME against latent embedding methods to evaluate the neighborhood structure preservation in the latent space. Considered methods for dimensionality reduction are PCA<sup>10</sup>, ISOMAP<sup>11</sup>, LLE<sup>12</sup> and p-UMAP<sup>13</sup>. As for ILLUME, the reduction methods are tested tuning the latent space dimension as hyperparameter from the list  $\{2, 4, 8, 16, 32\}$ . For p-UMAP, we train a 3-layer fully-connected neural network for 50 epochs. For the other methods, we used standard parameters.

**Experimental Setup for Local Explainers.** We compare ILLUME with well-known local explainers to evaluate the quality of explanations: LIME<sup>14</sup>, SHAP<sup>15</sup> for feature importance; LORE<sup>16</sup>, ANCHOR<sup>17</sup> for decision rules. LIME is tuned with neighborhood sizes  $\{100, 300, 1000, 5000\}$ ; LORE with sizes  $\{300, 1000\}$  and  $\{1, 5, 10\}$  decision trees; ANCHOR with batch sizes  $\{100, 300\}$  and beam sizes  $\{4, 10\}$ . With SHAP we use the kernelSHAP method for synthetic black-boxes and treeSHAP for ensemble black-boxes in real-world data.

**Experimental Setup for Global Surrogates.** Global surrogates models LR<sup>18</sup> and DT<sup>19</sup> are trained with latent or input space variables by tuning their main hyperparameters to maximize test set prediction accuracy. For surrogates based on LR (INP-LR and LIN-LR), as local explanation the –global– logistic coefficients  $\{\beta_1, \beta_2, \dots\}$  are weighted by the feature values of the specific instance (see model-intrinsic additive scores [96]), namely  $\psi_{i,j}^{\text{INP}} = \beta_j x_{i,j}$  and  $\psi_{i,j}^{\text{LIN}} = \sum_{r=1}^k \beta_r W_{j,r}^b x_{i,j}$ . For a fair comparison, we apply the latent search for maximizing surrogate fidelity also for LIN-LR and LIN-DT using distance

$$^8 d_{\cos}(\mathbf{u}, \mathbf{v}) = 1 - \frac{\mathbf{u} \cdot \mathbf{v}}{\|\mathbf{u}\| \cdot \|\mathbf{v}\|}$$

$$^9 d_{hmm}(\mathbf{u}, \mathbf{v}) = \sum_i 1[u_i \neq v_i]$$

<sup>10</sup><https://scikit-learn.org/stable/modules/generated/sklearn.decomposition.PCA.html>

<sup>11</sup><https://scikit-learn.org/stable/modules/generated/sklearn.manifold.Isomap.html>

<sup>12</sup><https://scikit-learn.org/stable/modules/generated/sklearn.manifold.LocallyLinearEmbedding.html>

<sup>13</sup>[https://umap-learn.readthedocs.io/en/latest/parametric\\_umap.html](https://umap-learn.readthedocs.io/en/latest/parametric_umap.html)

<sup>14</sup>[https://lime-ml.readthedocs.io/en/latest/lime.html#module-lime\\_tabular](https://lime-ml.readthedocs.io/en/latest/lime.html#module-lime_tabular)

<sup>15</sup><https://shap.readthedocs.io/en/latest/generated/shap.Explainer.html>

<sup>16</sup>[https://kdd-lab.github.io/LORE\\_sa/html/index.html](https://kdd-lab.github.io/LORE_sa/html/index.html)

<sup>17</sup><https://github.com/marcotcr/anchor>

<sup>18</sup>[https://scikit-learn.org/stable/modules/generated/sklearn.linear\\_model.LogisticRegression.html](https://scikit-learn.org/stable/modules/generated/sklearn.linear_model.LogisticRegression.html)

<sup>19</sup><https://scikit-learn.org/stable/modules/generated/sklearn.tree.DecisionTreeClassifier.html>

<sup>7</sup><https://archive.ics.uci.edu/ml/index.php>

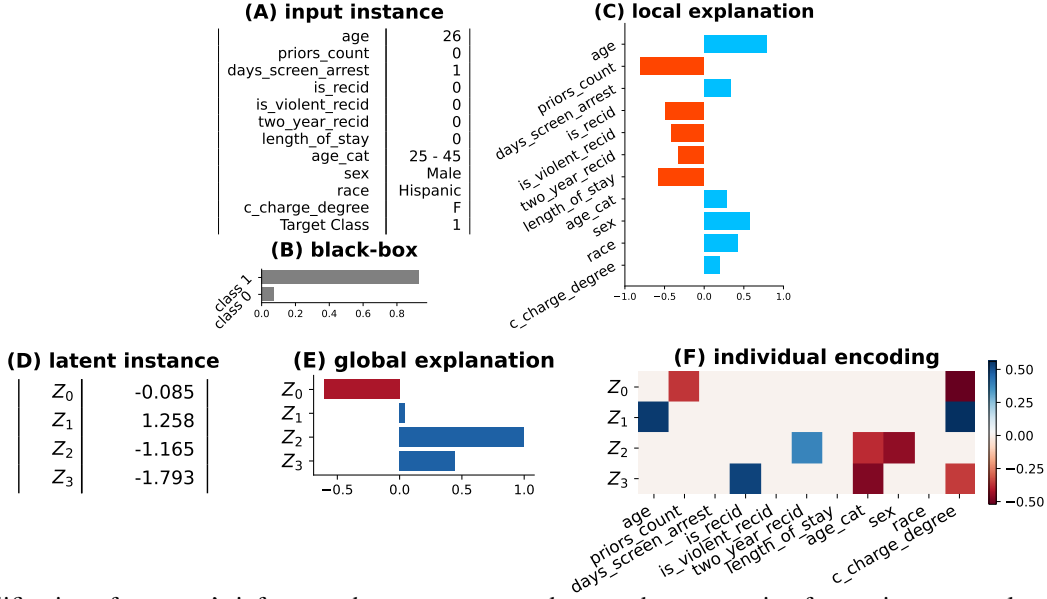


Fig. A1: Exemplification of ILLUME’s inference phase on *compas* dataset when generating feature importance local explanations. Given an input data-point  $\mathbf{x}_{test}$  (A) and its corresponding black-box prediction  $b(\mathbf{x}_{test})$  (B), the method outputs instance-specific explanation  $e_g(\mathbf{z}_{test}, \eta_{test}^b)$  (C). This explanation is derived: (i) by encoding the instance into a latent representation  $\mathbf{z}_{test}$  (D), (ii) extracting the logic of the global surrogate  $g$  (E), and (iii) combining it with local interpretable mapping  $\eta_{test}^b$  (F), represented by a sparse and linear transformation returned by the meta-encoder.

$d_Z$ . Instead, for LR and DT we search the nearest neighbor in the input space according to  $d_X$ . For remaining methods –LIME, SHAP, LORE and ANCHOR– we trust each explanation as valid one, since all these methods ensure guarantees for maximal fidelity.

### B. Qualitative Results

In Figure A1 it is illustrated how our approach works in the explanation inference phase with an example on *compas* dataset. Firstly, with ILLUME, instances and their local black-box decisions (A-B) are employed to generate local explanations (C). These explanations are computed with the information deriving from an auxiliary embedding space where we project the input (D). In this space we have extracted global latent explanations (E) during the surrogate learning process. The key component of this space is a set of instance-specific linear transformations (F) learned during the meta-encoder training process. Local explanations are produced by combining the latent explanation with the local projection of the data. Figure A2 showcase feature importance explanations for two neighboring instances from the *wine* dataset. Being closely located in the feature space and yielding similar predictions from the black-box model for the multi-class task, the explanations for these instances are expected to align, ranking important features in comparable ways. ILLUME demonstrates its ability to generate robust and consistent explanations, producing rank-preserving feature importance profiles for neighboring instances. In contrast, competing methods such as LIME and SHAP fail to achieve similar consistency. Additionally, Figure A3 presents a comparable example for decision rules using the same dataset, illustrating that ILLUME is capable of generating robust and consistent

rules. The similarity of these rules is evaluated using the *cplt-score*, like in the main experimental result of the paper. Furthermore, we demonstrate that ILLUME can produce more concise decision rules with respect to the analyzed competitors, a benefit achieved through sparsity regularization.

### C. Detailed Formulas for Decision Rules

In ILLUME, we first derive global explanations in the form of axis-parallel decision rules on latent features, determined by root-leaf paths in a trained decision tree, i.e.,  $\rho_i^z = \{z_{i,r} \in [l_r^z, u_r^z]\}_{r=1\dots k}$  (lower and upper bound are in the domain of  $z_{i,r}$ , extended with  $\pm\infty$ ). By exploiting the linearity of the mapping  $\eta_i^b$ , these rules are converted into input space local oblique rules  $\tilde{\rho}_i^x = \{\sum_{j=1}^m W_{i,j,r}^b x_{i,j} \in [l_r^z, u_r^z]\}_{r=1\dots k}$ . While oblique rules offer a valid and expressive form of explanation, for consistency with most methods we perform an additional step to convert the oblique rules into the standard axis-parallel format:  $\rho_i^x = \{x_{i,j} \in [l_{i,j}^x, u_{i,j}^x]\}_{j=1\dots m}$ . The upper and lower bounds for these axis-parallel rules are derived by isolating  $x_{i,j}$  to express the rule in terms of individual input features. For example, from the oblique rules  $\sum_{j=1}^m W_{i,j,r}^b x_{i,j} \geq l_r^z$  and  $\sum_{j=1}^m W_{i,j,r}^b x_{i,j} \leq u_r^z$ , it follows:

$$l_{i,j}^x = \max_r \frac{l_r^z - \sum_{v \neq j} W_{i,v,r}^b x_{i,v}}{W_{i,j,r}^b}$$

$$u_{i,j}^x = \min_r \frac{u_r^z - \sum_{v \neq j} W_{i,v,r}^b x_{i,v}}{W_{i,j,r}^b}.$$

The max/min operations ensure taking the most restrictive inequality among the  $k$  latent conditions, i.e., the largest lower bound and the smallest upper bound. Finally, exploiting the

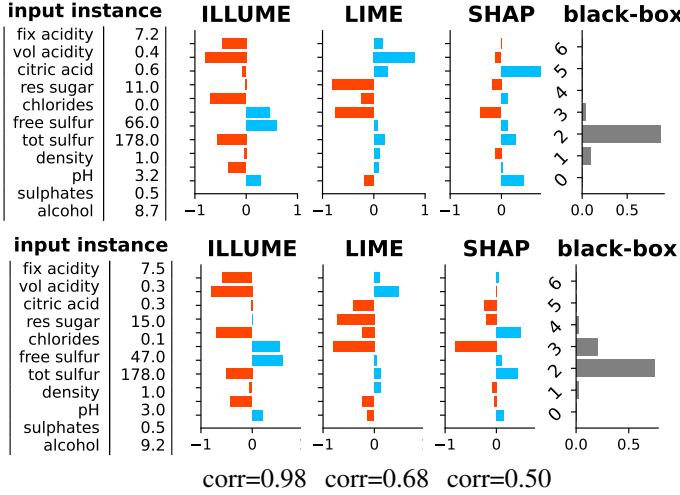


Fig. A2: Feature importance explanations for two similar records of the wine dataset. Feature values are reported on the left. In the center, explanations are derived with ILLUME, LIME and SHAP. On the right, the prediction probability returned by an XGB classifier.

equality  $z_{i,r} = \sum_{v \neq j} W_{i,v,r}^b x_{i,v} + W_{i,j,r}^b x_{i,j}$ , we find the relations reported in the main paper that link upper/lower bounds in the embedding and in the original space:

$$l_{i,j}^x - x_{i,j} = \max_r \frac{l_r^z - z_{i,r}}{W_{i,j,r}^b} \quad u_{i,j}^x - x_{i,j} = \min_r \frac{u_r^z - z_{i,r}}{W_{i,j,r}^b}.$$

#### D. Analysis of Stability Loss

Here, we provide an intuition behind the stability loss computation, which guarantees that small changes in the original data space lead to minimal perturbations in the latent space, thus ensuring a consistent and reliable mapping across data points. As described in Section III, we enforce each local transformation to remain valid when applied to slightly perturbed input. Specifically, omitting  $b$  for simplicity, if the encoding is given by  $\mathbf{z} = \eta(\mathbf{x}) = f(\mathbf{x}) \cdot \mathbf{x}$ , where  $f(\mathbf{x})$  represents the individual transformation for  $\mathbf{x}$ , then the same transformation must hold for a small perturbation  $\mathbf{x} + \delta$ . In other words, the encoding operates locally around the instance  $\mathbf{x}$  as a linear transformation characterized by a matrix  $f(\mathbf{x})$ , which is approximately constant within the neighborhood of  $\mathbf{x}$ . While the coefficients of the matrix dynamically adapt to the input, their rate of variation is slower than that of the input  $\mathbf{x}$ , ensuring stability and consistency of the transformation. This implies the following constraint:

$$\eta(\mathbf{x} + \delta) = f(\mathbf{x} + \delta) \cdot (\mathbf{x} + \delta) \approx f(\mathbf{x}) \cdot (\mathbf{x} + \delta).$$

We enforce this property by minimizing specific quantities which ensure the validity of the equation above. First, we show the first-order Taylor expansions of matrix entries of the local transformation  $f$  under small input perturbations:

$$f_{j,r}(\mathbf{x} + \delta) = f_{j,r}(\mathbf{x}) + \sum_{v=1}^m \frac{\partial f_{j,r}(\mathbf{x})}{\partial x_v} \delta_v + \mathcal{O}(\|\delta\|^2)$$

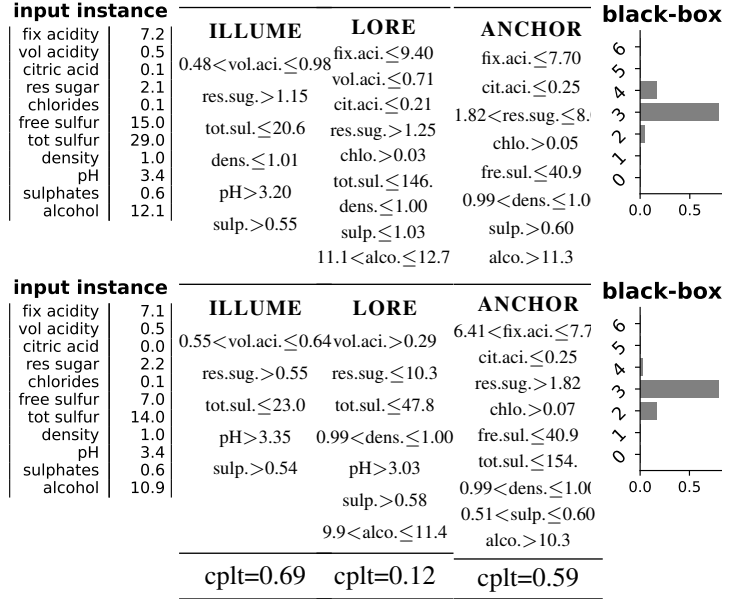


Fig. A3: Decision rule explanations for two similar records of the wine dataset. Feature values are reported on the left. In the center, explanations derived with ILLUME, LORE and ANCHOR. On the right, the prediction probability returned by an LGBM classifier.

Substituting these approximations into the expression for the encoding of the perturbation,  $\eta(\mathbf{x} + \delta) = f(\mathbf{x} + \delta) \cdot (\mathbf{x} + \delta)$ , for each entry of the vector we get (neglecting second-order terms):

$$\begin{aligned} \eta_r(\mathbf{x} + \delta) &\approx \sum_{j=1}^m \left( f_{j,r}(\mathbf{x}) + \sum_{v=1}^m \frac{\partial f_{j,r}(\mathbf{x})}{\partial x_v} \delta_v \right) (x_j + \delta_j) \\ &= \sum_{j=1}^m f_{j,r}(\mathbf{x}) (x_j + \delta_j) + \sum_{j=1}^m \left( \sum_{v=1}^m \frac{\partial f_{j,r}(\mathbf{x})}{\partial x_j} x_v \right) \delta_j + \mathcal{O}(\|\delta\|^2). \end{aligned}$$

Last equation tells us that describing the variation of the latent encoding  $\eta$ , when applied to a minimal perturbation of  $\mathbf{x}$ , requires the sum of two quantities (up to second-order corrections):

$$\eta(\mathbf{x} + \delta) \approx f(\mathbf{x})(\mathbf{x} + \delta) + D(\mathbf{x}) \cdot \delta \quad \left[ D_{j,r} = \sum_v \frac{\partial f_{v,r}}{\partial x_j} x_v \right]$$

The first term,  $f(\mathbf{x}) \cdot (\mathbf{x} + \delta)$ , represents the mapping of the perturbation  $\delta$  applied to the input  $\mathbf{x}$ , with the linear transformation  $f$  held constant. The second term,  $D(\mathbf{x}) \cdot \delta$ , captures the change in the transformation due to the perturbation  $\delta$  and its interaction with the input  $\mathbf{x}$ . Therefore, we enforce stability by minimizing  $\|D(\mathbf{x})\|_F^2$  during training. Reordering the terms  $\eta(\mathbf{x} + \delta) \approx f(\mathbf{x}) \cdot \mathbf{x} + (f(\mathbf{x}) + D(\mathbf{x})) \cdot \delta$ , we obtain the Taylor expansion of the encoding  $\eta$  under small input perturbations:

$$\eta(\mathbf{x} + \delta) \approx \eta(\mathbf{x}) + J(\mathbf{x}) \cdot \delta \quad \left[ J(\mathbf{x}) = f(\mathbf{x}) + D(\mathbf{x}) \right]$$

where we highlight the Jacobian matrix  $J$  around the data-point  $\mathbf{x}$ , with entries  $J_{j,r} = \frac{\partial \eta_r}{\partial x_j}$ . To minimize  $\|D(\mathbf{x})\|_F$ , we optimize the reported loss involving Jacobian matrix  $L^{st}(\mathbf{x}) = \|J(\mathbf{x}) - f(\mathbf{x})\|_F^2$  for each instance.



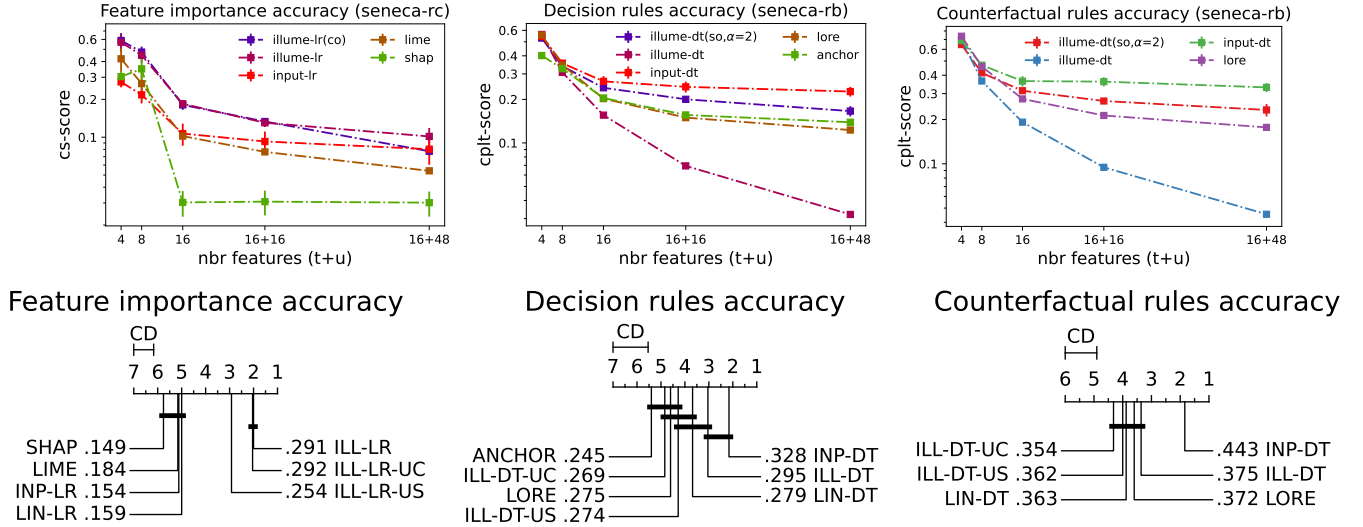


Fig. A4: Explanation accuracy for synthetic classifiers. In the Figures, average metrics for accuracy in feature importance and decision rules are reported varying the input feature size. In CD plots, average rankings for individual metrics are reported for different methods and datasets.

TABLE A2: Feature-based latent space quality metrics for all datasets and methods.

	Feature Preservation						KNN Gain					
	ILLUME-UC	LIN-UC	PCA	ISOMAP	LLE	UMAP	ILLUME-UC	LIN-UC	PCA	ISOMAP	LLE	UMAP
aids	.842	.851	1.000	.706	.527	.683	.946	.960	1.008	.896	.791	.895
austr	.852	.855	.993	.790	.612	.732	1.009	1.001	1.000	.984	.960	.984
bank	.845	.843	.952	.786	.594	.666	.963	.963	.959	.938	.990	.998
breast	1.000	.996	1.000	.928	.746	.849	1.000	1.010	1.000	1.001	1.001	1.001
churn	.908	.861	.919	.668	.521	.679	1.078	1.026	1.234	.977	.960	1.000
compas	.859	.870	1.000	.724	.563	.643	.985	.994	1.002	1.019	.976	1.020
ctg	.939	.927	1.000	.716	.635	.678	1.033	1.023	1.000	1.000	.996	.996
diabts	1.000	1.000	1.000	.845	.700	.792	1.019	1.000	1.000	.964	.848	.894
ecoli	1.000	1.000	1.000	.871	.806	.785	1.024	1.007	1.000	.977	.950	.961
fico	1.000	1.000	1.000	.832	.657	.680	1.006	1.003	1.000	.984	.964	.990
german	.849	.832	.945	.765	.589	.686	.994	.963	1.054	1.067	1.034	.992
home	1.000	1.000	1.000	.897	.679	.826	1.033	1.000	1.011	1.011	.956	.966
ionos	.994	.992	1.000	.868	.713	.749	1.053	1.045	1.052	1.006	1.004	1.006
sonar	.986	.967	.995	.871	.671	.800	1.003	.977	1.027	.890	.998	.946
spam	.921	.930	.953	.816	.585	.673	1.016	1.015	.994	.975	.924	.977
titnc	.868	.869	1.000	.896	.603	.797	1.047	1.047	1.000	1.014	.977	1.002
wine	1.000	1.000	1.000	.868	.670	.789	1.063	1.000	1.000	.974	.890	.933
yeast	.999	1.000	1.000	.887	.652	.799	.995	1.000	1.000	.965	.746	.870

### E. Detailed Experimental Results

Here, we report in details all the results that are shown in aggregated form in the main paper.

**RQ1: Goodness of Latent Space Quality.** In Tables A2, A3 and A4 are reported extensive results for all metrics, datasets and black-boxes that have been summarized with Table I in the main paper. In particular, central and right columns of Tables A3 and A4 report Macro-F1 accuracies for LR and DT trained on latent spaces both with and without black-box decision conditioning. The same results are aggregated and ranked in Figure A5. Firstly, we observe that models without conditioning consistently achieve lower accuracies in surrogate classification tasks. Secondly, particularly for the LR surrogate, ILLUME demonstrates significant improvements compared to LIN encodings. This underscores the importance of label conditioning, combined with using more expressive latent

features, in enhancing the accuracy of surrogate predictions.

**RQ2: Correctness for Synthetic Black-Box Explanations.** In Figure A4 we report additional results from synthetic black-box models. We also present preliminary results on generating **counterfactual explanations** using ILLUME. While decision rules are naturally derived from root-to-leaf paths in a decision tree, counterfactual rules are obtained through symbolic reasoning applied to the tree. Specifically, following the methodology in [8], we analyze the latent decision tree (the same one trained for decision rules) to identify all paths that lead to an opposite prediction compared to the input instance. By combining the split conditions from each of these paths, we retain only those counterfactuals that involve the minimal number of split conditions.

In the top pictures, we display with line plots the variation of explanation accuracy metrics with respect to the number



of input dimensions, comparing the best-regularized setup of ILLUME with the un-regularized one. For feature importance explanations, we observe that the non-collinear (*co*) regularizer slightly enhances the correctness of the explanations across most scenarios. However, in cases involving 16+48 input features, the explanation accuracy experiences a minor decline. In contrast, for both factual and counterfactual rules, the combination of sparsity ( $\alpha=2$ ) and soft-orthogonality (*so*) significantly improves the correctness of the explanations. These findings underscore the importance of consistently applying sparsity regularizers within ILLUME when generating rule-based explanations.

In the CD plots corresponding to the results presented in Table II of the main paper, we display aggregated rankings for each metric across all datasets. We observe the same trends as reported in the main paper: ILLUME and its variants perform similarly in terms of feature importance correctness, while ILLUME-DT shows comparable performance to INP-DT in factual rules correctness. Regarding counterfactual decision rules, there is no statistically significant difference between ILLUME-DT and LORE. However, INP-DT outperforms the others, consistent with its superior performance on factual rules.

### RQ3: Faithfulness and Robustness in Real-world Datasets.

Tables A5 and A6 present comprehensive results for feature importance metrics, while Tables A7 and A8 display detailed results for decision rules metrics. These tables include all datasets and black-box models that were summarized in Tables III and IV of the main paper.

Figure A6 presents additional findings that compare the effects of different regularizations on the robustness and faithfulness metrics for feature importance explanations. We observe that sparse regularizations (*so*,  $\alpha = 2$ ) do not enhance either robustness or faithfulness for feature importance. Additionally, models regularized for non-collinearity (*co*) perform similarly to unregularized models, although they achieve the highest average robustness scores. In contrast, Figures A7 show additional results comparing the impact of various regularizations on the robustness and faithfulness metrics for decision rules. Here, sparse regularizations (*so*,  $\alpha = 2$ ) significantly improve the quality of decision rules for both metrics, thereby confirming our earlier observations regarding sparsity and decision rule correctness. Overall, for both types of explanations, models optimized for stability and label conditioning perform significantly worse in terms of robustness and faithfulness, respectively.

Tables A9 and Tables A10 present additional results on explainers' **robustness** with the evaluation of a **global metric** rather than local metrics based on sensitivity to perturbations. Intuitively, a -globally-robust explainer should produce similar explanations for closely located data points – with the same back-box predicted label – and distinct explanations for those farther apart. Thus, robustness is assessed globally by calculating the Spearman's rank correlation coefficient between the pairwise distances of explanations,  $\{d_{\mathcal{E}}(i, j)\}_{i < j}$ , and the corresponding pairwise distances of input records,  $\{\|\mathbf{x}_i - \mathbf{x}_j\|_2\}_{i < j}$ , for those pairs of points with accordant

predicted labels. Like in SENECA, we use similarity metrics  $cs-score(\cdot, \cdot)$  and  $cplt-score(\cdot, \cdot)$  instead of distance metrics. Figure A8 also presents the aggregate performance of feature importance explainers. In this analysis, ILLUME-LR achieves the highest performance, while ILLUME-LR-US performs comparably. This is in contrast to the local robustness results reported in the main paper, where ILLUME-LR-US was significantly worse. Additionally, LIME demonstrates the poorest performance in this context, despite showing adequate local robustness in the main paper. Regarding decision rule explainers, LIN-LR experiences a decline in performance compared to the local robustness results and ranks similarly to both ILLUME-DT and ILLUME-DT-US.

TABLE A3: Decision-based latent space quality metrics with LGBM as black-box for all datasets and methods.

LGBM	Decision Preservation				LR Accuracy (Macro-F1)				DT Accuracy (Macro-F1)			
	ILLUME	LIN	ILLUME-UC	LIN-UNC	ILLUME	LIN	ILLUME-UC	LIN-UC	ILLUME	LIN	ILLUME-UC	LIN-UC
aids	<b>.618</b>	<u>.596</u>	.549	.555	<b>.952</b>	<u>.902</u>	.899	<u>.902</u>	<b>.930</b>	<u>.874</u>	.768	.780
austr	<b>.743</b>	<u>.729</u>	.613	.623	.920	<b>.927</b>	.919	<u>.920</u>	<u>.927</u>	<b>.942</b>	.869	.913
bank	<b>.659</b>	<u>.656</u>	.595	.588	<b>.901</b>	<u>.866</u>	.839	.840	<b>.881</b>	<b>.881</b>	<u>.759</u>	.736
breast	<b>.779</b>	<u>.739</u>	.728	.718	.981	<u>.990</u>	.981	<b>.991</b>	.972	.963	<u>.981</u>	<b>.991</b>
churn	<b>.610</b>	<u>.583</u>	.542	.548	<b>.875</b>	.637	<u>.650</u>	.623	<b>.852</b>	<u>.827</u>	.738	.760
compas	<b>.667</b>	<u>.665</u>	.644	.640	<b>.926</b>	.914	.902	<u>.914</u>	<b>.913</b>	<u>.893</u>	.891	.891
ctg	<b>.693</b>	<u>.689</u>	.624	.611	<u>.993</u>	<b>.996</b>	<b>.996</b>	<u>.993</u>	<u>.993</u>	<b>.996</b>	.969	.949
diabts	<b>.642</b>	<u>.640</u>	.621	.627	<b>.906</b>	.871	<u>.881</u>	.871	<b>.874</b>	.832	.836	<u>.864</u>
ecoli	<b>.726</b>	.700	<u>.706</u>	<u>.706</u>	<b>.970</b>	.936	<u>.947</u>	.936	<b>.939</b>	<b>.939</b>	.910	<u>.921</u>
fico	<b>.642</b>	.578	<u>.586</u>	.580	<b>.908</b>	.903	.894	<u>.903</u>	.862	<b>.869</b>	.843	.854
german	<b>.669</b>	<u>.627</u>	.566	.557	<u>.814</u>	.807	<b>.816</b>	.806	<b>.805</b>	<u>.791</u>	.699	.707
home	<b>.677</b>	<u>.626</u>	.614	.614	<u>.949</u>	<b>.949</b>	<b>.949</b>	<b>.949</b>	<b>.970</b>	.939	.929	<u>.949</u>
ionos	<u>.631</u>	<b>.665</b>	.586	.597	.886	<u>.906</u>	<b>.934</b>	.854	.919	<u>.952</u>	<b>.968</b>	.907
sonar	<b>.671</b>	<u>.629</u>	.576	.610	<b>.904</b>	<u>.857</u>	.810	.833	<b>.881</b>	<u>.833</u>	.785	.786
spam	<b>.704</b>	.647	<u>.674</u>	.623	<b>.963</b>	<u>.942</u>	<u>.942</u>	.936	<b>.955</b>	<u>.946</u>	.913	.903
titnc	<u>.743</u>	<b>.744</b>	.650	.672	.885	<b>.893</b>	<b>.893</b>	.885	<b>.937</b>	.919	.922	<u>.931</u>
wine	<b>.550</b>	<u>.546</u>	.536	.540	<b>.305</b>	.266	<u>.292</u>	.286	<u>.516</u>	<b>.537</b>	.497	.440
yeast	<b>.630</b>	.615	.609	<u>.623</u>	<b>.629</b>	.565	<u>.612</u>	.572	<b>.556</b>	<u>.534</u>	.525	.512

TABLE A4: Decision-based latent space quality metrics with XGB as black-box for all datasets and methods.

XGB	Decision Preservation				LR Accuracy (Macro-F1)				DT Accuracy (Macro-F1)			
	ILLUME	LIN	ILLUME-UC	LIN-UC	ILLUME	LIN	ILLUME-UC	LIN-UC	ILLUME	LIN	ILLUME-UC	LIN-UC
aids	<b>.661</b>	<u>.610</u>	.563	.557	<b>.941</b>	.871	<u>.880</u>	.868	<b>.938</b>	<u>.877</u>	.730	.774
austr	<u>.739</u>	<b>.751</b>	.657	.652	<b>.934</b>	<u>.913</u>	.912	.912	<b>.941</b>	<u>.911</u>	.898	.898
bank	<u>.653</u>	<b>.662</b>	.593	.582	<b>.893</b>	<u>.868</u>	.832	.853	<b>.886</b>	<u>.873</u>	.750	.744
breast	<b>.821</b>	.737	<u>.775</u>	.730	<u>.981</u>	<b>.990</b>	<u>.981</u>	<b>.990</b>	<u>.972</u>	<u>.972</u>	.961	<b>1.000</b>
churn	<b>.602</b>	<u>.587</u>	.536	.541	<b>.872</b>	<u>.660</u>	.649	.644	<b>.852</b>	<u>.786</u>	.728	.728
compas	<u>.671</u>	<b>.673</b>	.640	.638	<b>.933</b>	<u>.915</u>	.911	<u>.915</u>	<b>.915</b>	<u>.912</u>	.891	.888
ctg	<b>.743</b>	<u>.739</u>	.653	.629	<b>1.000</b>	<u>.996</u>	<u>.996</u>	<u>.996</u>	<u>.957</u>	.945	<b>1.000</b>	.945
diabts	<b>.684</b>	<u>.649</u>	.625	.626	<b>.910</b>	.871	<u>.879</u>	.871	<u>.857</u>	<b>.895</b>	.849	<u>.857</u>
ecoli	<u>.721</u>	.703	<b>.726</b>	.709	<b>1.000</b>	.969	<u>.988</u>	.980	<u>.980</u>	<b>.992</b>	.947	<u>.980</u>
fico	<b>.650</b>	.588	<u>.592</u>	.588	<b>.937</b>	<u>.929</u>	.922	<u>.929</u>	<u>.886</u>	<b>.897</b>	.882	.874
german	<b>.655</b>	<u>.617</u>	.535	.516	<u>.789</u>	<b>.810</b>	.761	.778	<u>.780</u>	<b>.791</b>	.714	.697
home	<b>.663</b>	<u>.642</u>	.630	.626	<u>.939</u>	<b>.949</b>	.939	<u>.939</u>	<u>.929</u>	<b>.970</b>	.939	.929
ionos	.566	<b>.603</b>	<u>.575</u>	.572	<u>.891</u>	.868	<b>.904</b>	.883	.874	<b>.954</b>	<u>.936</u>	.880
sonar	<u>.619</u>	<b>.629</b>	.595	<b>.629</b>	.786	.785	.810	<b>.833</b>	<b>.857</b>	.762	<u>.786</u>	.762
spam	<b>.721</b>	.667	<u>.675</u>	.631	<b>.968</b>	<u>.947</u>	.942	.940	<b>.966</b>	<u>.952</u>	.919	.901
titnc	<b>.725</b>	.687	.655	.694	<u>.877</u>	<b>.890</b>	.883	.877	<b>.923</b>	<u>.921</u>	<u>.921</u>	.910
wine	<b>.587</b>	<u>.574</u>	.562	.566	<b>.334</b>	.276	<u>.319</u>	.287	.422	<b>.544</b>	.441	<u>.494</u>
yeast	<b>.700</b>	<u>.695</u>	.690	.694	<b>.790</b>	.755	<u>.776</u>	.752	<u>.676</u>	<b>.698</b>	.644	.656

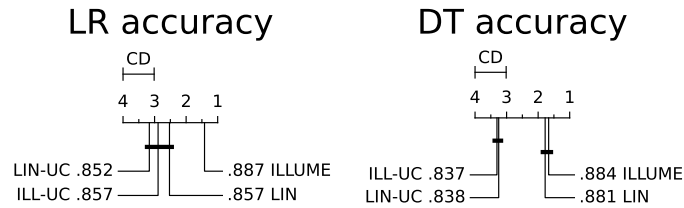


Fig. A5: Critical Difference plots with Nemenyi test at 90% confidence level for prediction accuracy metrics in real-world datasets, comparing LR and DT performances over different training feature spaces.

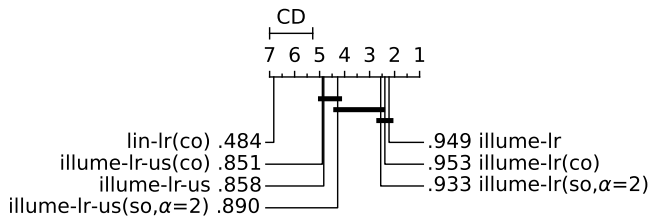
TABLE A5: Robustness and faithfulness metrics for feature importance methods in all datasets with LGBM as black-box. Prediction accuracy of surrogate classifiers is reported inside parentheses.

LGBM	Feature Importance Robustness						Feature Importance Faithfulness					
	ILLUME-LR	ILLUME-LR-US	LIN-LR	INP-LR	LIME	SHAP	ILLUME-LR	ILLUME-LR-UC	LIN-LR	INP-LR	LIME	SHAP
aids	<b>.994</b> (95.3)	.797 (97.0)	.582 (93.7)	.244 (93.7)	<u>.978</u>	.445	<b>.908</b> (97.4)	.234 (93.5)	.540 (93.5)	.610 (93.7)	.054	<u>.806</u>
austr	<b>.980</b> (93.5)	.901 (89.9)	.659 (92.0)	.500 (92.0)	<u>.904</u>	.443	.785 (92.0)	.520 (92.0)	.561 (89.9)	.659 (92.0)	.033	<b>.798</b>
bank	<b>.994</b> (96.1)	<u>.958</u> (96.0)	.536 (94.9)	.271 (95.0)	.916	.127	<b>.790</b> (96.8)	.304 (95.4)	.537 (95.0)	<u>.540</u> (95.0)	.122	.410
breast	.777 (98.2)	<u>.811</u> (97.4)	.388 (99.1)	.219 (98.2)	<b>.964</b>	.328	.846 (99.1)	<u>.859</u> (98.2)	.819 (97.4)	<u>.833</u> (98.2)	.113	<b>.906</b>
churn	<b>.981</b> (95.8)	<u>.932</u> (94.8)	.719 (87.3)	.672 (87.6)	.618	.160	<b>.679</b> (96.6)	.142 (89.1)	.055 (87.4)	.247 (87.6)	.091	<u>.644</u>
compas	<b>.993</b> (94.7)	.711 (95.1)	.711 (94.4)	.635 (94.4)	<u>.971</u>	.538	<b>.798</b> (95.8)	.317 (94.0)	.319 (94.4)	.313 (94.4)	.015	<u>.448</u>
ctg	<b>.980</b> (99.8)	<u>.840</u> (99.8)	.758 (99.5)	.617 (99.3)	.781	.656	<b>.741</b> (99.8)	.357 (99.5)	.624 (99.5)	.519 (99.3)	.487	<u>.682</u>
diabts	<u>.966</u> (92.9)	.797 (94.2)	.180 (89.6)	.176 (89.6)	<b>.985</b>	.163	.396 (92.9)	.298 (90.9)	<u>.454</u> (89.6)	.450 (89.6)	.021	<b>.580</b>
ecoli	.958 (100.)	<u>.961</u> (100.)	.735 (100.)	.673 (100.)	<b>.981</b>	.585	<b>.640</b> (100.)	.623 (100.)	.575 (100.)	.586 (100.)	.260	<u>.503</u>
fico	<b>.981</b> (90.3)	.899 (90.8)	.400 (90.3)	.324 (90.3)	<u>.918</u>	.268	<u>.443</u> (91.4)	.338 (89.5)	.379 (90.3)	.377 (90.3)	.000	<b>.600</b>
german	<b>.996</b> (89.0)	<u>.930</u> (85.5)	.394 (85.5)	.338 (88.5)	.840	.069	<b>.531</b> (87.5)	.198 (88.0)	.174 (85.5)	.190 (88.5)	.124	<u>.238</u>
home	.878 (96.0)	.756 (97.0)	.204 (94.9)	.122 (94.9)	<b>.976</b>	.178	.741 (97.0)	.337 (94.9)	.495 (94.9)	.486 (94.9)	.077	<b>.752</b>
ionos	<u>.845</u> (94.4)	.688 (94.4)	.371 (88.7)	.353 (88.7)	<b>.932</b>	.366	.385 (93.0)	.153 (94.4)	.568 (91.5)	<u>.576</u> (88.7)	.193	<b>.841</b>
sonar	.621 (85.7)	<u>.698</u> (92.9)	.104 (83.3)	.085 (83.3)	<b>.914</b>	.078	.211 (90.5)	.055 (88.1)	.201 (88.1)	.077 (83.3)	.032	<b>.469</b>
spam	<b>.923</b> (96.0)	<u>.859</u> (96.2)	.396 (94.0)	.311 (94.4)	.808	.166	<b>.848</b> (96.4)	.441 (94.5)	.522 (94.6)	.037 (94.4)	.000	<u>.662</u>
titnc	<b>.991</b> (90.5)	<u>.919</u> (90.5)	.616 (89.9)	.646 (89.4)	.971	.536	<b>.769</b> (91.6)	.640 (90.5)	.639 (89.9)	.641 (89.4)	.389	<u>.733</u>
wine	<b>.943</b> (64.2)	<u>.640</u> (67.2)	.192 (59.1)	.176 (58.6)	.779	.166	<b>.152</b> (72.3)	.105 (62.8)	.135 (58.8)	<u>.146</u> (58.6)	.022	.104
yeast	<b>.934</b> (76.4)	<u>.705</u> (75.1)	.323 (69.4)	.305 (69.4)	.289	.128	<b>.280</b> (78.5)	.143 (74.1)	.216 (70.7)	<u>.217</u> (69.4)	.018	.177

TABLE A6: Robustness and faithfulness metrics for feature importance methods in all datasets with XGB as black-box. Prediction accuracy of surrogate classifiers is reported inside parentheses.

XGB	Feature Importance Robustness						Feature Importance Faithfulness					
	ILLUME-LR	ILLUME-LR-US	LIN-LR	INP-LR	LIME	SHAP	ILLUME-LR	ILLUME-LR-UC	LIN-LR	INP-LR	LIME	SHAP
aids	<b>.994</b> (95.3)	.901 (95.1)	.505 (91.1)	.328 (91.1)	<u>.965</u>	.393	<b>.838</b> (95.8)	.252 (91.8)	.654 (91.1)	.574 (91.1)	.083	<u>.799</u>
austr	<b>.987</b> (92.0)	.872 (92.8)	.614 (90.6)	.514 (90.6)	<u>.929</u>	.341	<b>.783</b> (94.2)	.560 (91.3)	.704 (90.6)	.698 (90.6)	.000	<u>.737</u>
bank	<b>.989</b> (96.2)	<u>.929</u> (96.0)	.503 (95.3)	.260 (95.5)	.910	.213	<b>.826</b> (97.1)	.397 (94.9)	.352 (93.8)	.473 (95.5)	.269	<u>.765</u>
breast	.875 (99.1)	.803 (99.1)	.451 (100.)	.502 (97.4)	<b>.970</b>	.302	.888 (98.2)	.883 (98.2)	.850 (98.2)	.864 (97.4)	.128	<b>.927</b>
churn	<b>.974</b> (95.1)	<u>.840</u> (95.1)	.776 (88.0)	.680 (87.9)	.549	.163	<b>.612</b> (95.8)	.128 (89.1)	.154 (88.5)	.197 (87.9)	.078	<u>.611</u>
compas	<b>.989</b> (95.4)	.742 (95.2)	.713 (94.5)	.597 (94.5)	<u>.971</u>	.532	<b>.731</b> (96.1)	.320 (94.4)	.330 (94.5)	.321 (94.5)	.004	<u>.525</u>
ctg	<b>.992</b> (100.)	<u>.859</u> (99.8)	.670 (99.8)	.477 (99.8)	.824	.502	<b>.776</b> (100.)	.323 (99.8)	.688 (99.8)	.434 (99.8)	.066	<u>.696</u>
diabts	<u>.971</u> (92.2)	.780 (92.9)	.225 (90.3)	.208 (87.0)	<b>.984</b>	.171	.390 (92.9)	.273 (90.3)	<u>.517</u> (89.0)	.507 (87.0)	.048	<b>.671</b>
ecoli	<u>.973</u> (100.)	.945 (100.)	.722 (100.)	.659 (98.5)	<b>.990</b>	.726	<b>.720</b> (100.)	.711 (100.)	.683 (100.)	.691 (98.5)	.358	<u>.516</u>
fico	<b>.973</b> (93.4)	.944 (93.2)	.433 (92.9)	.368 (92.9)	<u>.971</u>	.304	<u>.516</u> (95.3)	.409 (92.3)	.453 (92.9)	.450 (92.9)	.000	<b>.672</b>
german	<b>.996</b> (87.0)	<u>.953</u> (87.0)	.512 (86.0)	.320 (86.0)	.782	.071	<b>.492</b> (89.0)	.131 (86.5)	.167 (82.5)	.200 (86.0)	.005	<u>.358</u>
home	<u>.956</u> (93.9)	.912 (96.0)	.162 (93.9)	.141 (93.9)	<b>.974</b>	.148	.636 (97.0)	.277 (94.9)	.474 (93.9)	.470 (93.9)	.027	<b>.712</b>
ionos	<u>.772</u> (91.5)	.734 (91.5)	.382 (87.3)	.351 (90.1)	<b>.950</b>	.322	.244 (97.2)	.189 (91.5)	.533 (88.7)	<u>.551</u> (90.1)	.162	<b>.914</b>
sonar	.784 (81.0)	.686 (81.0)	.090 (76.2)	.069 (78.6)	<b>.935</b>	.168	.183 (83.3)	.137 (83.3)	.124 (81.0)	.084 (78.6)	.042	<b>.633</b>
spam	<b>.912</b> (96.5)	.819 (96.9)	.291 (94.5)	.141 (94.6)	<u>.878</u>	.140	<b>.823</b> (97.0)	.462 (94.5)	.421 (94.6)	.265 (94.6)	.013	<u>.721</u>
titnc	<b>.993</b> (91.1)	.921 (91.1)	.662 (89.4)	.608 (89.9)	<u>.973</u>	.633	.571 (90.5)	.671 (89.9)	.638 (88.8)	.634 (89.9)	.155	<b>.809</b>
wine	<b>.952</b> (66.3)	.581 (66.6)	.183 (60.4)	.174 (59.3)	<u>.856</u>	.278	<b>.223</b> (72.9)	.165 (64.3)	.206 (60.1)	<u>.209</u> (59.3)	.042	.107
yeast	<b>.964</b> (86.5)	.795 (88.2)	.391 (81.5)	.394 (81.8)	<u>.941</u>	.813	<b>.528</b> (88.2)	.353 (84.2)	.325 (81.5)	.311 (81.8)	.152	<u>.290</u>

Feature importance robustness



Feature importance faithfulness

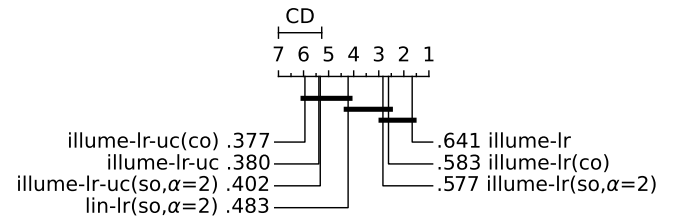


Fig. A6: Critical Difference plots with Nemenyi test at 90% confidence level for robustness and faithfulness metrics in real-world datasets, comparing various regularized versions of ILLUME-LR.

TABLE A7: Robustness and faithfulness metrics for decision rules methods in all datasets with LGBM as black-box. Prediction accuracy of surrogate classifiers is reported inside parentheses.

LGBM	Decision Rule Robustness						Decision Rule Faithfulness					
	ILLUME-DT	ILLUME-DT-US	LIN-DT	INP-DT	LORE	ANCHOR	ILLUME-DT	ILLUME-DT-UC	LIN-DT	INP-DT	LORE	ANCHOR
aids	.676 (97.4)	.301 (96.7)	<b>.911</b> (97.9)	.486 (98.8)	.060	.180	.739 (97.4)	.644 (96.5)	<b>.825</b> (97.9)	.804 (98.8)	.762	<b>.868</b>
austr	.404 (92.0)	.438 (92.0)	<b>.573</b> (97.1)	.288 (94.9)	.147	.218	<b>.707</b> (92.0)	.653 (94.9)	<b>.694</b> (97.1)	.661 (94.9)	.666	.672
bank	.595 (95.5)	.504 (95.5)	<b>.679</b> (95.3)	<b>.600</b> (96.1)	.038	.053	.642 (95.5)	.566 (93.8)	<b>.734</b> (95.3)	<b>.675</b> (96.1)	.510	.457
breast	.352 (98.2)	.114 (96.5)	<b>.452</b> (98.2)	<b>.536</b> (96.5)	.077	.025	<b>.863</b> (98.2)	.788 (98.2)	<b>.817</b> (96.5)	.736 (96.5)	.735	.381
churn	<b>.618</b> (95.7)	.471 (95.2)	<b>.890</b> (97.3)	.358 (98.2)	.215	.099	<b>.609</b> (95.7)	.399 (91.6)	.560 (97.3)	<b>.605</b> (98.2)	.605	.413
compas	<b>.603</b> (95.1)	.351 (94.3)	<b>.961</b> (95.1)	.361 (95.8)	.115	.168	.584 (95.1)	.564 (94.5)	<b>.619</b> (95.1)	.536 (95.8)	.503	<b>.592</b>
ctg	.791 (99.3)	.677 (99.3)	<b>.975</b> (99.3)	<b>.866</b> (99.3)	.317	.031	.777 (99.3)	<b>.779</b> (99.1)	.743 (99.3)	<b>.839</b> (99.3)	.666	.335
diabts	.116 (89.6)	.057 (87.7)	<b>.166</b> (89.6)	.098 (88.3)	.047	.097	.449 (89.6)	<b>.545</b> (90.9)	.344 (89.6)	.295 (88.3)	.276	<b>.646</b>
ecoli	<b>.632</b> (100.)	.569 (100.)	<b>.784</b> (100.)	.529 (100.)	.478	.462	.570 (100.)	<b>.587</b> (100.)	.531 (100.)	.513 (100.)	.541	<b>.600</b>
fico	<b>.673</b> (90.1)	.262 (89.5)	<b>.390</b> (89.5)	.200 (90.5)	.038	.167	<b>.512</b> (90.1)	<b>.425</b> (89.4)	<b>.512</b> (89.5)	.481 (90.5)	.457	<b>.637</b>
german	<b>.618</b> (86.0)	.287 (85.5)	<b>.562</b> (83.0)	.154 (81.0)	.058	.085	<b>.327</b> (86.0)	.142 (87.0)	.112 (83.0)	.141 (81.0)	.118	<b>.369</b>
home	.064 (96.0)	.058 (96.0)	.051 (98.0)	<b>.150</b> (94.9)	.014	<b>.073</b>	<b>.511</b> (96.0)	.420 (97.0)	.469 (98.0)	.485 (94.9)	.407	<b>.680</b>
ionos	<b>.438</b> (98.6)	.297 (97.2)	<b>.570</b> (95.8)	.376 (95.8)	.204	.155	<b>.793</b> (98.6)	.722 (97.2)	<b>.751</b> (95.8)	.697 (95.8)	.748	.645
sonar	.194 (83.3)	.147 (85.7)	<b>.515</b> (81.0)	.398 (83.3)	.108	.043	<b>.458</b> (85.7)	.444 (85.7)	<b>.422</b> (81.0)	<b>.453</b> (83.3)	.214	.441
spam	.402 (96.1)	<b>.459</b> (95.1)	<b>.652</b> (94.5)	.249 (93.7)	.120	.113	<b>.767</b> (95.1)	.622 (92.8)	<b>.701</b> (94.5)	.642 (93.7)	.253	.495
titnc	.628 (93.9)	.476 (95.0)	<b>.948</b> (96.1)	<b>.687</b> (94.4)	.288	.420	.762 (95.0)	.748 (96.1)	<b>.792</b> (96.1)	.702 (94.4)	.697	<b>.795</b>
wine	<b>.296</b> (72.2)	.230 (70.1)	<b>.525</b> (70.6)	.154 (70.2)	.134	.224	.097 (72.2)	.087 (71.4)	.099 (70.6)	.108 (70.2)	<b>.214</b>	<b>.388</b>
yeast	<b>.568</b> (78.5)	.471 (77.8)	<b>.713</b> (76.4)	.362 (78.5)	.467	.418	.412 (78.5)	.367 (77.8)	.274 (75.4)	.319 (78.5)	<b>.427</b>	.358

TABLE A8: Robustness and faithfulness metrics for decision rules methods in all datasets with XGB as black-box. Prediction accuracy of surrogate classifiers is reported inside parentheses.

XGB	Decision Rule Robustness						Decision Rule Faithfulness					
	ILLUME-DT	ILLUME-DT-US	LIN-DT	INP-DT	LORE	ANCHOR	ILLUME-DT	ILLUME-DT-UC	LIN-DT	INP-DT	LORE	ANCHOR
aids	<b>.666</b> (95.6)	.378 (93.0)	<b>.798</b> (94.2)	.098 (95.1)	.023	.153	.642 (95.6)	.518 (93.7)	<b>.657</b> (94.2)	.645 (95.1)	.639	<b>.821</b>
austr	<b>.513</b> (92.0)	.387 (92.8)	<b>.713</b> (92.8)	.262 (89.9)	.123	.256	<b>.780</b> (92.8)	.691 (90.6)	<b>.587</b> (92.8)	.591 (89.9)	.697	<b>.751</b>
bank	<b>.620</b> (95.9)	.528 (95.5)	<b>.767</b> (94.9)	.549 (95.1)	.022	.047	<b>.728</b> (95.9)	.539 (95.6)	.551 (94.9)	<b>.743</b> (95.1)	.360	.465
breast	.243 (96.5)	.184 (96.5)	<b>.465</b> (97.4)	<b>.563</b> (96.5)	.068	.032	<b>.813</b> (96.5)	<b>.772</b> (97.4)	.769 (97.4)	.795 (96.5)	.703	.374
churn	.291 (96.1)	<b>.625</b> (94.5)	<b>.895</b> (95.8)	.355 (99.0)	.229	.112	.517 (96.1)	.365 (93.4)	.504 (95.8)	<b>.571</b> (99.0)	<b>.533</b>	.394
compas	<b>.811</b> (94.0)	.448 (94.2)	<b>.965</b> (94.5)	.385 (94.6)	.101	.154	<b>.606</b> (94.2)	.523 (93.4)	.576 (94.5)	.506 (94.6)	.489	<b>.592</b>
ctg	.869 (99.8)	.852 (100.)	<b>.976</b> (99.5)	<b>.882</b> (99.5)	.340	.033	<b>.787</b> (100.)	.727 (99.3)	.722 (99.5)	<b>.795</b> (99.5)	.654	.347
diabts	.124 (91.6)	.062 (90.3)	.124 (90.9)	<b>.176</b> (92.2)	.044	<b>.177</b>	.532 (91.6)	<b>.563</b> (92.2)	.503 (90.9)	.411 (92.2)	.293	<b>.688</b>
ecoli	<b>.680</b> (100.)	.533 (100.)	<b>.800</b> (100.)	.588 (100.)	.581	.497	<b>.748</b> (100.)	.673 (100.)	<b>.753</b> (100.)	.666 (100.)	.623	.562
fico	.340 (93.8)	.279 (92.1)	<b>.413</b> (92.8)	.221 (93.8)	.053	.187	.617 (93.8)	.632 (93.0)	.614 (92.8)	.628 (93.8)	<b>.643</b>	<b>.679</b>
german	<b>.337</b> (87.0)	.129 (82.5)	<b>.565</b> (81.5)	.107 (83.5)	.033	.081	<b>.226</b> (87.0)	.169 (81.0)	.052 (81.5)	.041 (83.5)	.098	<b>.388</b>
home	<b>.095</b> (96.0)	.037 (96.0)	.082 (97.0)	<b>.132</b> (94.9)	.010	.062	<b>.578</b> (96.0)	.414 (97.0)	.555 (97.0)	.488 (94.9)	.455	<b>.730</b>
ionos	.385 (95.8)	.374 (94.4)	<b>.514</b> (97.2)	<b>.615</b> (97.2)	.212	.232	<b>.701</b> (95.8)	.683 (95.8)	<b>.790</b> (97.2)	<b>.829</b> (97.2)	.710	.730
sonar	.211 (85.7)	.221 (85.7)	<b>.533</b> (88.1)	<b>.254</b> (92.9)	.141	.072	<b>.546</b> (85.7)	<b>.597</b> (85.7)	.324 (88.1)	.535 (92.9)	.427	.516
spam	.419 (96.1)	<b>.483</b> (97.1)	<b>.699</b> (94.6)	.403 (94.7)	.130	.090	<b>.797</b> (97.1)	.643 (93.1)	.663 (94.6)	<b>.675</b> (94.7)	.227	.478
titnc	.620 (95.5)	.469 (95.0)	<b>.955</b> (97.2)	.693 (96.1)	.387	.463	<b>.819</b> (95.5)	.690 (97.2)	.781 (97.2)	.737 (96.1)	.738	<b>.807</b>
wine	<b>.303</b> (71.0)	.244 (71.0)	<b>.458</b> (70.6)	.162 (68.2)	.150	.229	.160 (71.0)	.148 (71.5)	.164 (70.6)	.145 (68.2)	<b>.298</b>	<b>.403</b>
yeast	<b>.533</b> (89.2)	.437 (89.9)	<b>.788</b> (88.2)	.427 (89.9)	.469	.387	<b>.590</b> (89.9)	.469 (87.5)	.470 (88.2)	.538 (89.9)	<b>.613</b>	.361

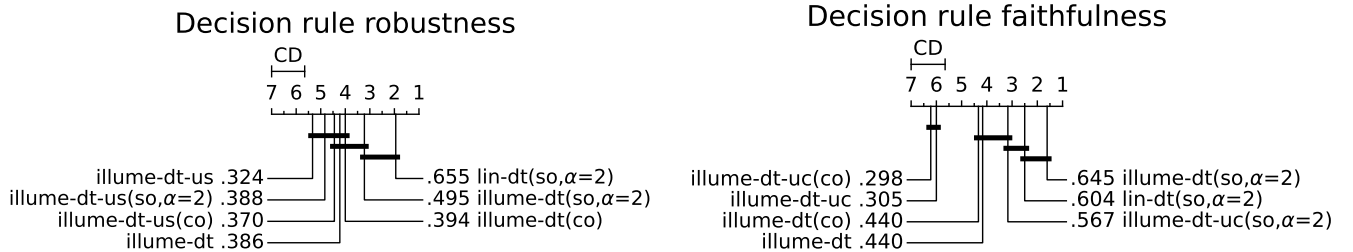


Fig. A7: Critical Difference plots with Nemenyi test at 90% confidence level for robustness and faithfulness metrics in real-world datasets, comparing various regularized versions of ILLUME-DT.

TABLE A9: Global robustness metrics in all datasets with LGBM as black-box. Prediction accuracy of surrogate classifiers is reported inside parentheses.

LGBM	Feature Importance Robustness						Decision Rule Robustness					
	ILLUME-LR	ILLUME-LR-US	LIN-LR	INP-LR	LIME	SHAP	ILLUME-DT	ILLUME-DT-UC	LIN-DT	INP-DT	LORE	ANCHOR
aids	<b>.743</b> (95.3)	<u>.653</u> (97.0)	<u>.563</u> (93.7)	<u>.352</u> (93.7)	.163	.254	<u>.267</u> (97.4)	<u>.252</u> (96.7)	<b>.595</b> (97.9)	.192 (98.8)	.170	.191
australian	<b>.801</b> (93.5)	<u>.651</u> (89.9)	<u>.488</u> (92.0)	<u>.396</u> (92.0)	.041	.181	<u>.297</u> (91.3)	<b>.383</b> (92.0)	<u>.361</u> (97.1)	.274 (94.9)	.197	.141
bank	<b>.897</b> (96.1)	<u>.839</u> (96.0)	<u>.798</u> (94.9)	<u>.671</u> (95.0)	.147	.298	<b>.540</b> (95.5)	<u>.387</u> (95.5)	<u>.425</u> (95.3)	.192 (96.1)	.055	.066
breast	<u>.532</u> (97.4)	<b>.638</b> (96.5)	<u>.568</u> (99.1)	<u>.553</u> (98.2)	.280	.226	<b>.285</b> (98.2)	<u>.266</u> (96.5)	.227 (96.5)	.123 (96.5)	.024	.122
churn	<b>.664</b> (95.8)	<u>.655</u> (94.8)	<u>.614</u> (87.0)	<u>.476</u> (87.6)	.000	.299	<b>.350</b> (95.7)	<u>.256</u> (95.2)	.210 (97.3)	.167 (98.2)	.138	.100
compas	<b>.875</b> (94.7)	<u>.685</u> (95.1)	<u>.527</u> (94.4)	<u>.421</u> (94.4)	.142	.352	<u>.432</u> (95.1)	<b>.547</b> (94.3)	<u>.493</u> (95.1)	.205 (95.8)	.193	.152
ctg	<b>.758</b> (99.8)	<u>.729</u> (99.8)	<u>.732</u> (99.5)	<u>.647</u> (99.3)	.117	.405	<u>.293</u> (99.3)	<u>.445</u> (99.3)	<b>.511</b> (99.3)	.062 (99.3)	.011	.275
diabts	<b>.700</b> (92.9)	<u>.684</u> (94.2)	<u>.499</u> (89.6)	<u>.498</u> (89.6)	.486	.335	<u>.305</u> (89.6)	<u>.304</u> (87.7)	.255 (89.6)	<b>.344</b> (88.3)	.198	.231
ecoli	<u>.825</u> (100.)	<b>.871</b> (100.)	<u>.834</u> (100.)	<u>.838</u> (100.)	.447	.749	<u>.524</u> (100.)	<b>.653</b> (100.)	.451 (100.)	.277 (100.)	.456	<b>.633</b>
fico	<b>.744</b> (90.3)	<u>.678</u> (90.8)	<u>.501</u> (90.3)	<u>.426</u> (90.3)	.415	.411	<b>.318</b> (90.1)	<u>.300</u> (89.5)	.274 (89.5)	.224 (90.5)	.131	.247
german	<b>.736</b> (89.0)	<u>.653</u> (85.5)	<u>.559</u> (85.5)	<u>.523</u> (88.5)	.072	.242	<u>.243</u> (86.0)	<u>.252</u> (85.5)	<b>.354</b> (83.0)	.214 (81.0)	.193	.251
home	<b>.720</b> (96.0)	<u>.612</u> (97.0)	<u>.606</u> (94.9)	<u>.590</u> (94.9)	.437	.311	<u>.478</u> (96.0)	<u>.341</u> (96.0)	.430 (98.0)	<b>.510</b> (94.9)	.434	<u>.449</u>
ionosphere	<b>.741</b> (94.4)	<u>.740</u> (94.4)	<u>.723</u> (88.7)	<u>.519</u> (88.7)	.259	.586	<u>.524</u> (98.6)	<u>.341</u> (90.1)	.581 (95.8)	.144 (95.8)	.054	.212
sonar	<b>.793</b> (85.7)	<u>.735</u> (92.9)	<u>.725</u> (83.3)	<u>.715</u> (83.3)	.288	.388	<b>.581</b> (83.3)	<u>.382</u> (85.7)	.379 (81.0)	.228 (83.3)	.129	.102
spam	<u>.386</u> (96.0)	.178 (96.2)	<b>.416</b> (94.0)	<u>.357</u> (94.4)	.274	.069	.201 (94.7)	<u>.273</u> (95.1)	.152 (94.5)	.097 (93.7)	.147	<b>.289</b>
titnc	<b>.864</b> (90.5)	.770 (90.5)	<u>.777</u> (89.9)	<u>.689</u> (89.4)	.551	.681	.612 (93.9)	<u>.616</u> (95.0)	<b>.658</b> (96.1)	.569 (94.4)	.470	.548
wine	<b>.714</b> (64.2)	<u>.602</u> (67.2)	<u>.577</u> (59.1)	<u>.554</u> (58.6)	.243	.484	<u>.269</u> (72.2)	<u>.271</u> (70.1)	.225 (70.6)	.253 (70.2)	.270	<b>.359</b>
yeast	<b>.617</b> (76.4)	<u>.474</u> (75.1)	<u>.436</u> (69.4)	<u>.440</u> (69.4)	.096	.299	<u>.331</u> (78.5)	<u>.355</u> (77.8)	<u>.380</u> (75.4)	<u>.376</u> (78.5)	.248	<b>.411</b>

TABLE A10: Global robustness metrics in all datasets with XGB as black-box. Prediction accuracy of surrogate classifiers is reported inside parentheses.

XGB	Feature Importance Robustness						Decision Rule Robustness					
	ILLUME-LR	ILLUME-LR-US	LIN-LR	INP-LR	LIME	SHAP	ILLUME-DT	ILLUME-DT-UC	LIN-DT	INP-DT	LORE	ANCHOR
aids	<b>.720</b> (95.3)	<u>.492</u> (95.1)	<u>.485</u> (91.1)	<u>.400</u> (91.1)	.159	.250	<u>.298</u> (95.6)	<b>.400</b> (92.3)	.249 (94.2)	.196 (95.1)	.194	.186
australian	<b>.781</b> (92.0)	<u>.482</u> (92.8)	<u>.554</u> (90.6)	<u>.569</u> (90.6)	.022	.269	<b>.378</b> (92.0)	<u>.377</u> (92.8)	.291 (92.8)	.193 (89.9)	.262	.262
bank	<b>.872</b> (96.2)	<u>.810</u> (96.0)	<u>.758</u> (95.3)	<u>.668</u> (95.5)	.105	.293	<b>.530</b> (95.9)	<u>.496</u> (95.5)	.436 (94.9)	.145 (95.1)	.012	.055
breast	<u>.698</u> (99.1)	<b>.707</b> (99.1)	<u>.506</u> (100.0)	<u>.272</u> (97.4)	.262	.251	<u>.305</u> (96.5)	<b>.356</b> (95.6)	.295 (97.4)	.183 (96.5)	.127	.108
churn	<u>.585</u> (95.1)	<b>.648</b> (95.1)	<u>.604</u> (87.6)	<u>.473</u> (87.9)	.017	.339	<u>.324</u> (96.1)	<b>.326</b> (94.5)	.315 (95.8)	.192 (99.0)	.132	.175
compas	<b>.844</b> (95.4)	<u>.713</u> (95.2)	<u>.589</u> (94.5)	<u>.407</u> (94.5)	.127	.354	<u>.327</u> (94.0)	<u>.546</u> (94.2)	<b>.552</b> (94.5)	.179 (94.6)	.162	.137
ctg	<b>.811</b> (100.)	<u>.776</u> (99.8)	<u>.760</u> (99.8)	<u>.552</u> (99.8)	.000	.545	<u>.402</u> (99.8)	.390 (100.)	<b>.405</b> (99.5)	.081 (99.5)	.000	.271
diabts	<b>.661</b> (92.2)	<u>.620</u> (92.9)	<u>.487</u> (90.3)	<u>.486</u> (87.0)	.600	.380	<u>.278</u> (91.6)	<u>.271</u> (90.3)	<b>.307</b> (90.9)	<u>.281</u> (92.2)	<b>.307</b>	.239
ecoli	<b>.892</b> (100.)	<u>.851</u> (100.)	<u>.811</u> (100.)	<u>.816</u> (98.5)	.381	.662	<u>.466</u> (100.)	<b>.723</b> (100.)	<u>.551</u> (100.)	.288 (100.)	.527	.587
fico	<b>.718</b> (93.4)	<u>.674</u> (93.2)	<u>.519</u> (92.9)	<u>.342</u> (92.9)	.432	.371	<b>.346</b> (93.8)	<u>.326</u> (92.1)	.234 (92.8)	.197 (93.8)	.108	.236
german	<b>.714</b> (87.0)	<u>.629</u> (87.0)	<u>.640</u> (86.0)	<u>.541</u> (86.0)	.054	.315	<u>.270</u> (87.0)	.209 (77.5)	<b>.403</b> (81.5)	.195 (83.5)	.160	.261
home	<b>.729</b> (93.9)	<u>.671</u> (96.0)	<u>.618</u> (93.9)	<u>.613</u> (93.9)	.611	.355	<b>.506</b> (96.0)	<u>.408</u> (96.0)	<u>.452</u> (97.0)	<u>.473</u> (94.9)	.407	.457
ionosphere	<u>.678</u> (91.5)	<b>.741</b> (91.5)	<u>.733</u> (87.3)	<u>.479</u> (90.1)	.235	.216	<b>.718</b> (95.8)	<u>.647</u> (94.4)	.456 (97.2)	.090 (97.2)	.086	.120
sonar	<u>.723</u> (81.0)	<b>.756</b> (81.0)	<u>.671</u> (76.2)	<u>.673</u> (78.6)	.062	.325	<u>.391</u> (85.7)	<b>.496</b> (85.7)	.259 (88.1)	.283 (92.9)	.138	.027
spam	<u>.577</u> (96.5)	<b>.579</b> (96.9)	<u>.425</u> (94.5)	<u>.279</u> (94.6)	.351	.069	<u>.234</u> (95.9)	<b>.238</b> (97.1)	.173 (94.6)	.046 (94.7)	.132	.232
titnc	<b>.830</b> (91.1)	<u>.704</u> (91.1)	<u>.682</u> (88.8)	<u>.710</u> (89.9)	.433	.588	<u>.621</u> (95.5)	<u>.642</u> (95.0)	<b>.661</b> (97.2)	.594 (96.1)	.550	.541
wine	<b>.667</b> (66.3)	<u>.629</u> (66.6)	<u>.616</u> (60.4)	<u>.563</u> (59.3)	.338	.485	<u>.286</u> (71.0)	.285 (71.0)	.253 (70.6)	.262 (68.2)	.273	<b>.347</b>
yeast	<b>.644</b> (86.5)	<u>.637</u> (88.2)	<u>.503</u> (81.5)	<u>.472</u> (81.8)	.314	.412	<u>.385</u> (89.2)	<u>.425</u> (89.9)	<u>.434</u> (88.2)	<b>.448</b> (89.9)	.329	.436

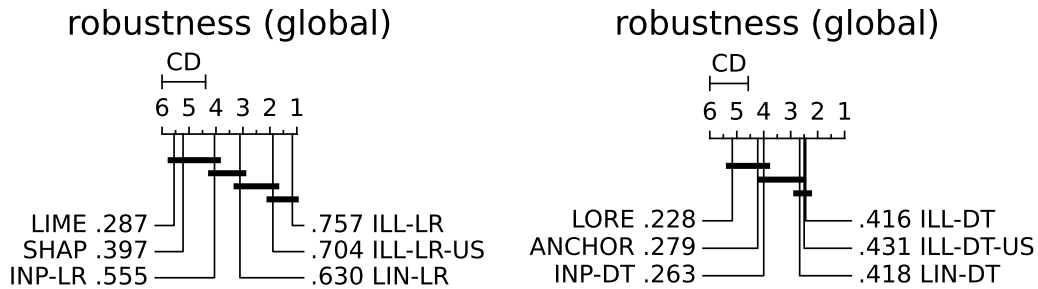


Fig. A8: Critical Difference plots with Nemenyi test at 90% confidence level for global robustness metrics in real-world datasets.